UNIVERSITY OF OKLAHOMA

GRADUATE COLLEGE

SCALE FORMATION IN POROUS MEDIA AND ITS IMPACT ON OIL RECOVERY

A THESIS

SUBMITTED TO THE GRADUATE FACULTY

in partial fulfillment of the requirements for the

Degree of

MASTER OF SCIENCE

By

SASSAN HAJIREZAIE
Norman, Oklahoma
2016

SCALE FORMATION IN POROUS MEDIA AND ITS IMPACT ON OIL RECOVERY

A THESIS APPROVED FOR THE
MEWBOURNE SCHOOL OF PETROLEUM AND GEOLOGICAL ENGINEERING

BY

_____
Dr. Xingru Wu, Chair

_____
Dr. Maysam Pournik

_____
Dr. Mashhad Fahes

Dedication

To my mother, father, brother and sister.

Acknowledgements

I would like to thank Dr. Wu, Dr. Pournik and Dr. Fahes for their technical guidance, friendship and support of my research.

Table of Contents

List of Tables

List of Figures

Abstract

The objectives of this study include: (1) investigation of the chemical and thermodynamic mechanisms of scale formation in porous media and its impact on formation damage; (2) development of a model to predict permeability and porosity reduction resulting from scale deposition in porous media; (3) quantification of the impact of scale formation within reservoir on oil recovery and injectivity loss; (4) examining the impact of scale formation on water flooding efficiency in terms of water saturation profiles and evaluating the effect of composite scale formation in porous media on reservoir properties.

Scale formation in oil fields has been repeatedly reported as the main issue affecting water flooding projects. Scale formation occurs both in reservoir porous media and within the operation facilities. In porous media, permeability and porosity tend to change because of scale formation. In oil fields, water injection can drop from thousands barrel per day to zero in one day because of scale formation during field operations. Therefore, prediction of scale formation and evaluating its impact on production performance is of vital importance for the oil industry.

In this research, scale formation in reservoir porous media and its impact on reservoir performance during water flooding are investigated. First, mineral deposition is studied from a micro scale (pore scale) standpoint and next, the impact of deposition on reservoir performance is studied on a macro scale basis.

A robust model is developed to predict permeability damage resulting from scale deposition in porous media. Results indicate that the solubility of minerals and the

amount of fluid that is injected into porous media have the most impact on formation damage of a reservoir.

In addition, a synthetic field operation is simulated in this work to study the impact of scale formation on injection and production performance during water flooding. The simulation results show that scale formation leads in the loss of injectivity and a reduction in the ultimate oil recovery. Moreover, saturation profiles indicate that scaling issue within reservoir leads in non-ideal displacement for water flooding.

Chapter 1: Introduction

1.1: Introduction to scale formation in oil fields

Scale formation is a common issue in oil and gas industry and it usually occurs during water flooding processes. When the injected water is not compatible with the formation water, scale formation would occur. For example, seawaters are usually rich in anions such as sulfate and carbonate while formation waters are usually rich in cations such as barium and calcium. Mixing these waters may lead to mineral scale deposition such as barium sulfate and calcium carbonate. Other types of scaling which have been observed in oil fields include calcium sulfate, strontium sulfate, Strontium Sulfate, Zinc/Lead and Iron Sulfide Scales.

Different parameters have been known to impact mineral nucleation and scale formation. Temperature, pressure, the rate of injected water, solubility, the properties of porous media and molality of ions are among these parameters.

Scale formation has been mainly studied in wellbores where engineers can observe the depositions. However, scale formation starts to occur in the reservoir porous media where the depositions plug the pore bodies and throats, which results in reservoir storability and transmissibility reduction. The mechanism of scale formation from supersaturated fluids and scale deposition in wellbore and facilities have been well studied while fewer studies have been focused on scaling in reservoir formation.

Development of models as well as designing experiments to study scale deposition in reservoir porous media and investigating its impact on reservoir performance is of vital importance. Microscopic study of scale formation in porous media is vital. Mineral

nucleation and precipitation highly depends on the size of the pore bodies and throats where the chemical reaction is occurring. It is more probable for the ions to collide in smaller pores while there are fewer collisions in the larger pores and therefore, fewer chances for scale nucleation and formation. In addition, the thickness of scales in pore bodies and throats defines the amount of damage on the storability and transmissibility of the pore network.

On the other hand, the impact of scale formation in porous media on oil fields can be captured from a macroscopic standpoint. Scale formation significantly affects the success of a water flooding project. Field cases have shown that ignoring the scaling issue can lead in significant losses of injectivity and productivity and therefore, care should be taken before designing water flooding projects.

1.2: Research Objectives

This research attempts to study in-situ scale formation by addressing the following objectives:

- Development of a model for predicting permeability impairment resulting from scale formation in porous media
- Modification of Carman-Kozeny equation for developing a pore scale relationship between porosity and permeability when mineral deposition has occurred in porous media
- Quantification of the impact of scale formation on water saturation profiles and water flooding efficiency
- Investigation of the impact of single barite and composite barite/calcium sulfate scaling on injectivity and oil recovery

1.3: Layout of Chapters

Chapter 2 presents the fundamentals of scale formation and reviews related literature. Various types of scale are introduced and relevant parameters are defined and discussed. In addition, various models and experimental procedures and their results as well as a few field cases are presented in this chapter.

Chapter 3 describes micro scale modeling of scale formation in porous media. Various parameters that affect scale deposition are studied and multivariate regression analysis is utilized to develop a model for predicting the permeability damage resulting from mineral scale formation in reservoir porous media. In order to validate the model, experimental data from the literature along with various statistical and graphical analyses are employed. In addition, Carman-Kozeny model is used to develop a modified model for representing the relationship between porosity and permeability when the porous medium is affected by scaling issue.

Chapter 4 investigates the injection of seawater rich in sulfate into a reservoir rich in barium to simulate a synthetic oil field affected by barium sulfate (barite) scale deposition within the reservoir. The impacts of barite scale formation on reservoir porosity and permeability are investigated in this chapter. This chapter also presents the impact of barite scale formation on injection performance and oil recovery. In addition, sensitivity analysis is performed based on the reactive surface area of barite. Moreover, calcium sulfate scale is added to barite scale to investigate the impact of composite scale formation on reservoir properties and injection performance.

The impact of scale formation on water flooding efficiency is presented in this chapter as well. Water saturation profiles are employed to quantify the effect of mineral deposition on the displacement behavior of water injection. In addition, a brief description of barite scale formation and reactive surface area of minerals is provided in this chapter.

Chapter 5 briefly summarizes the key points of the research along with the corresponding conclusions. In addition, a few recommendations are suggested for future works.

Chapter 2: Scale Formation in Oil Fields- Fundamentals and Literature Review

Waterflooding is one the the most widely used methods to maintain the depleted reservoir pressure and enhance oil recovery. However, inorganic scale formation occurs when the injected and formation waters are incompatible. Incompatibility means that while chemically interacting with each other, the waters precipitate minerals. Scale formation occurs all the way from the reservoir porous media up to the surface through pipelines and facilities. The different locations where scale formation occurs and the main reasons for each of them are reported in the literature [1].

Seawaters as the main sources for injection have high concentrations of anions such as SO_4^{-2} while formation waters are usually rich in cations such as Ca^{2+}, Ba^{2+} and Sr^{2+}. Mixing these incompatible or chemically different waters leads to precipitation of minerals such as $CaSO_4$, $BaSO_4$ and $SrSO_4$ during water flooding processes. A complete list of the composition of seawaters and formation waters are reported in the literature [2]. Precipitation of minerals occurs when the concentration of solute exceeds its solubility under specific thermodynamic condition.

2.1: Various Types of Scale Formation

Several types of scales form in oil fields. These scales include calcium carbonate ($CaCO_3$), calcium sulfate ($CaSO_4$), barium sulfate ($BaSO_4$) and strontium sulfate ($SrSO_4$). The most common oilfield scales and their causes have been reported in the literature [2]. Here, a brief summary about these scales is provided.

2.1.1: Calcium Carbonate Scales

When pressure drops, CO_2 comes out of the produced water and causes water pH and saturation index of carbonate minerals to increase and thus precipitation occurs.

The most common calcium carbonate scale type, which occurs in oilfield production operations, is calcite because it is more stable than other types of calcium carbonate such as aragonite and vaterite. The governing equation for calcium carbonate precipitation is as follows:

$$Ca^{2+} + CO_3^{2-} \Leftrightarrow CaCO_3 \quad (1)$$

Carbonate ion is rarely present in waters and thus most of the calcium carbonate scales result from decomposition of calcium bicarbonate based on the following reaction:

$$Ca(HCO_3)_2 \Leftrightarrow CaCO_3 + CO_2 + H_2O \quad (2)$$

Since CO_2 is released from the water as a result of pressure reduction (in chokes and separators), the above reaction proceeds to the right and thus calcium carbonate precipitates once its amount becomes more than what the water can dissolve.

2.1.2: Calcium Sulfate Scales

Another type of scale formation that causes severe formation damage and flow assurance issues is calcium sulfate. It has three different crystalized forms known as gypsum ($CaSO_4.2H_2O$), hemihydrate ($CaSO_4.1/2H_2O$) and anhydrate ($CaSO_4$). Gypsum is the most common calcium sulfate scale type at low temperatures. At temperatures above 100ºC, anhydrate is the stable form of calcium sulfate scale. Hemihydrate scale formation occurs at temperatures between 100 to 121ºC in brines with high ionic

strength and in non-turbulent environments. The general reaction for calcium sulfate precipitation is as follows:

$$Ca^{2+} + SO_4^{2-} \Leftrightarrow CaSO_4 \quad (3)$$

Calcium sulfate scales have been reported to have a decreasing solubility trend when temperature increases. In addition, they precipitate more in acidic environments.

Injection of two incompatible waters including calcium and sulfate into the Berea sandstones has shown that pressure has a small impact on $CaSO_4$ precipitation while at higher flow velocities, brine supersaturation and temperature have large impacts on the $CaSO_4$ precipitation. In addition, a model has been developed for predicting precipitation in the Berea sandstones at given temperature, injection velocity and brine supersaturation [3]. Figure 2- 1 shows the impact of temperature on the solubility of $CaSO_4$ as well as other important scales.

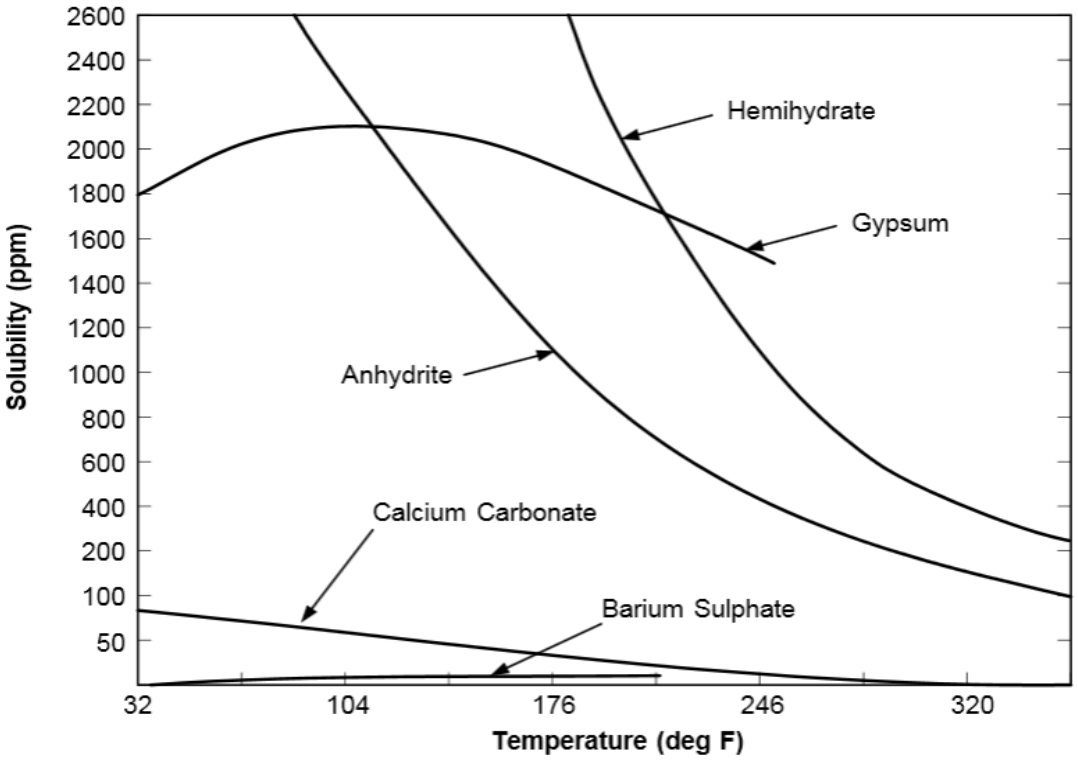

Figure 2- 1: Solubility of various scales as a function of temperature. Most scales are less soluble as temperature increases while barium sulfate is more soluble by increasing temperature [2].

2.1.3: Barium Sulfate Scales

Barium Sulfate is probably the most insoluble type of scales. Barium sulfate scale occurs both in porous media and wellbore. Once it precipitates and forms scale, its removal is very difficult. Therefore, care should be taken prior to its crystallizations and scale formation by using squeeze inhibitors. The governing equation for barium sulfate is as follows:

$$Ba^{2+} + SO_4^{2-} \Leftrightarrow BaSO4 \quad (4)$$

Experimental tests on barite scaling in both beakers and sandpacks have shown that the permeability reduction is mainly influenced by the crystal growth of barite instead of flow blockage and particle transport. Moreover, the precipitation process in porous media is dominated by the heterogeneous nucleation while the barium concentration in sandpack tests is less than that of beaker tests. In addition, it has been observed that the first contact point of incompatible brines consists of the highest amount of precipitation [4].

Core flooding tests on the West Africa offshore reservoir samples at atmospheric pressure and ambient temperature and constant injection velocity have shown that by evaluating the amount of barite precipitation by means of sulfate and barium profiles, for a seawater containing less sulfate, the scaling tendency tends to reduce which has been verified by the results of SEM analysis [5].

In addition to the single barite scaling, the impact of various parameters including calcium ion concentration, temperature and the size of deposited scales on composite $CaSO_4$-$BaSO_4$ scale deposition has been studied. It has been shown that by increasing temperature, co-precipitation of $CaSO_4$ and $BaSO_4$ increases and thus, more permeability reduction will occur. However, temperature has an opposite effect on single $BaSO_4$ precipitation. It has been proposed that small amounts of $CaSO_4$ along with $BaSO_4$ significantly reduce the permeability compared with the case in which only single $CaSO_4$ scale exists [6].

2.1.4: Strontium Sulfate Scales

Strontium sulfate has a similar behavior to barium sulfate but is more soluble and thus causes less severe scales. In most of oilfields, whenever barium sulfate scale occurs, strontium sulfate scaling is present as well. The governing equation for strontium sulfate is as follows:

$$Sr^{2+} + SO_4^{2-} \Leftrightarrow BaSO4 \quad (5)$$

Moreover, prediction of different sulfate scales including barium, calcium and strontium sulfates has been studied by considering the impact of temperature, pressure and water composition. The results indicate that the least soluble scales such as barium sulfate precipitate first and remove some sulfate ions from the solution leaving less anions for other cations to react with. Because of this phenomenon, the activity product required for forming the new scales should be modified [7].

2.1.5: Zinc/Lead and Iron Sulfide Scales

Zinc sulfide scale occurs when the formation water containing zinc mixes with the H_2S gas in wells and causes this type of precipitation. Several sources have been reported for zinc and lead ions, including precipitations that occur when connate water and aquifer water mix and the zinc ions that are introduced to the formation from the completion fluid during drilling and work over processes. Reservoir H_2S gas has been reported to be the main source of sulfide ion.

When the injected water containing dissolved H_2S reacts with formation water containing iron (specially, in sandstone formations), iron sulfide is precipitated based on the following equation:

$$Fe^{2+} + H_2S \Leftrightarrow FeS + 2H^{+} \quad (6)$$

Another source of iron is well tubular. Iron sulfide has been reported to occur in oil and gas wells, sour wells and water injectors where there are high amounts of sulfate in the water.

2.2: Important Parameters Affecting Scale Formation

Several reasons have been reported in the literature for scale formation [8]. The most important parameters include: pressure, temperature, cumulative volume of injection fluid, the concentration of ions in the injected fluid, precipitation reaction rate and crystal growth rate, pore size distribution, fluid dynamics in porous media, porous media surface properties. Crystallization induction time, initial porosity and permeability of the media, velocity of the injected fluid, physical changes in fluid properties due to crystallization, diffusion and mass transfer have been known as other important factors for scale formation.

In the following section, a brief description of the impact of some of the mentioned parameters on different types of scale precipitation is summarized [2]:

2.2.1: Effect of Supersaturation

Once the concentration of minerals in a solution exceeds the equilibrium concentration, precipitation starts to take place and as a result, different types of scales form in both porous media and wellbore tubing. In fact, supersaturation condition is dependent on several other parameters including pressure, temperature, concentration of ions, pH, etc.

Scaling index is the criterion for evaluating the scaling tendency, which will be discussed later.

2.2.2: Effect of Pore Size Distribution and Upscaling Chemical Reactions

Scale formation is highly influenced by the scale of medium in which it is studied. These medium scales vary from pore scales to field scales. Three main reasons that inhibit nucleation in small pores are summarized as follow:

1: Nucleation is a stochastic process in which the random collisions of the ions lead in formation of clusters. In the smaller pores, the probability of these collisions is less as the number of ions present in the smaller pores is less.

2: The crystal growth is limited by the small size of the pore and also, there is a possibility that a supersaturated solution in larger pores could be undersaturated in smaller pores.

3: The pore surface plays an important role in precipitation proposing that a favorable surface chemistry can promote the nucleation process [9].

By using scanning electron microscopy (SEM) and conducting experimental tests on sandstone and limestone samples, it has been found that precipitations mainly plugs the pore throats especially in limestone samples. Also, a linear relationship exists between the permeability reduction and the precipitations occupying the pore throats [10]. It has been found that the large crystals of scales plug the pores while being perpendicular to the rock surface [11]. Researchers are now able to observe the scaling phenomenon

from the nucleation stage to the complete pore plugging stage as can be observed in Figure 2- 2.

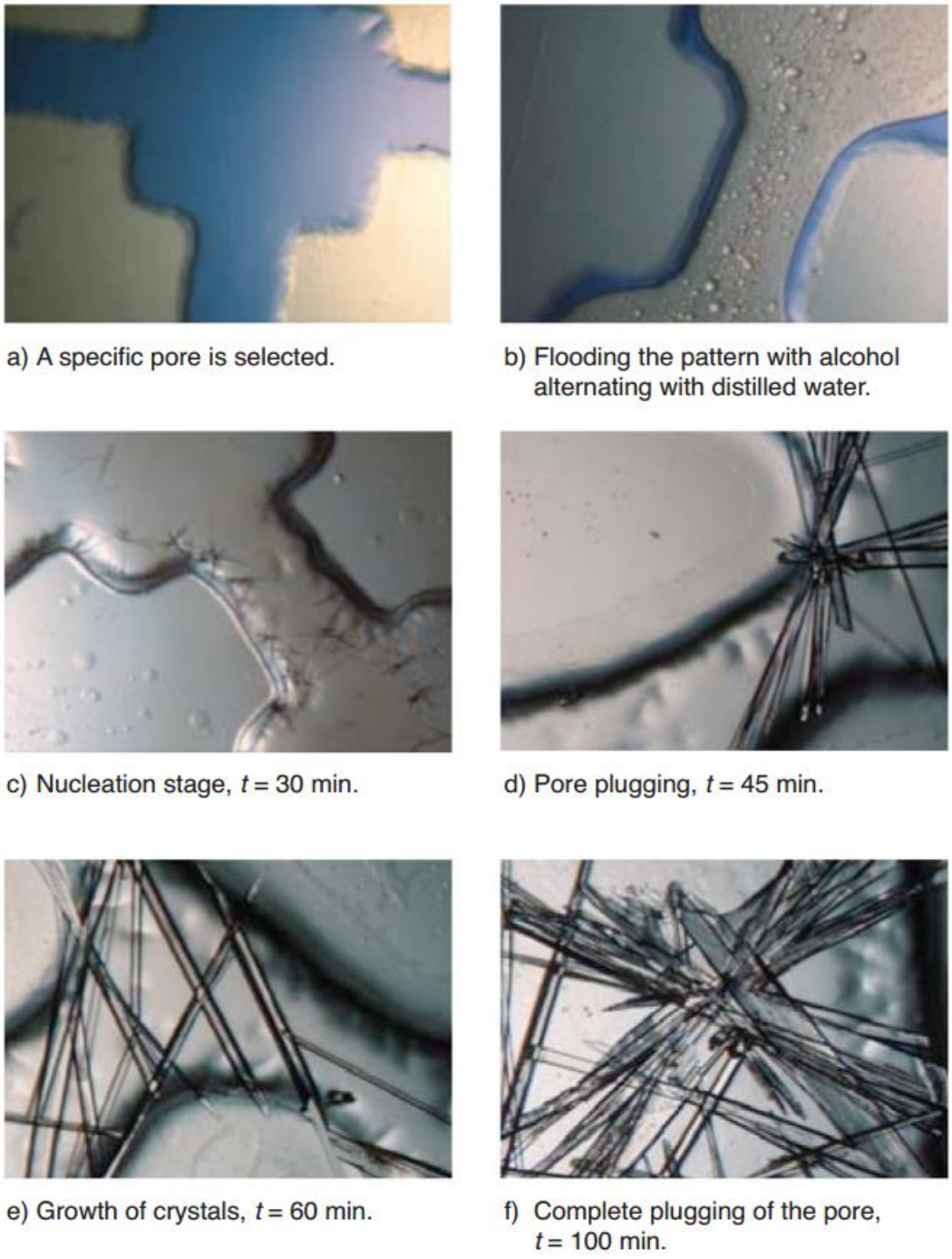

Figure 2- 2: Different stages of $CaSO_4$ precipitation [12]

Chemical reaction rates are usually measured in lab and then used in the reactive transport models for predicting the reaction and transport of species in porous media. However, the heterogeneities in porous media cause some errors when using these experimentally measured reaction rates for predications. Therefore, upscaling the reaction rates are of importance. The impact of scaling is small when the concentrations of species are small in pores. However, simulations show that where the pore scale concentrations of reactive species and the reaction rates vary spatially, the impact of scaling is large. Therefore, appropriate scaling approaches are vital for effectively capturing the impact of porous media heterogeneities on chemical reaction properties involved in mineral deposition [13].

2.2.3: Effect of Temperature

Temperature has different impacts on different scaling as shown in Figure 2- 1. Calcium sulfate and calcium carbonate scaling tendency increases by increasing temperature. Strontium sulfate has a similar behavior when temperature increases. Barium sulfate shows a different behavior when temperature varies. An increase in temperature leads to a stronger ionic strength of barium sulfate brine and thus, a decrease in scaling tendency of barium sulfate.

Studies show that the impact of temperature on salt precipitation resulting from CO_2 injection into reservoirs is small compared to the impacts of pressure and salinity. At higher pressures (up to 24 MPa), salt precipitation increases by increasing temperature (35-60^{0}C) while at lower pressures (8.5 MPa), this trend is opposite. Therefore, the impact of temperature on salt precipitation during CO_2 injection is pressure dependent.

However, the impact of temperature on salt precipitation is small compared to the impact of brine salinity and the relative permeability of the aqueous phase [14].

2.2.4: Effect of Pressure

The solubility of calcium, barium and strontium sulfates increases by increasing pressure and therefore, scale formation occurs more likely when pressure drops. This condition considerably occurs in perforations and in chokes as well as the production tubing. Calcium carbonate solubility is highly affected by the CO_2 content of water. An increase in CO_2 partial pressure reduces calcium carbonate precipitation.

2.3: Thermodynamics and Chemistry of Scale Formation

Scale formation tendency is evaluated by saturation index defined as follows [15]:

$$SI \equiv Log_{10}\left\{\frac{activityproduct}{K_{eq}}\right\} \tag{7}$$

As an example, for calcite, which forms based on the following reaction:

$$Ca^{2+} + CO_3^{2-} \rightarrow CaCO_3 \tag{8}$$

the saturation index would be:

$$SI_{Calcite} = Log_{10}\left[\frac{(a_{Ca^{2+}})\,(a_{CO_3^{2-}})}{K_{eq}}\right] = Log_{10}\left[\frac{[Ca^{2+}][CO_3^{2-}](\gamma_{Ca^{2+}})(\gamma_{CO_3^{2-}})}{K_{eq}}\right] \tag{9}$$

In this equation $[Ca^{2+}]$ stands for molality of calcium in mol/kg. K_{eq} is the equilibrium constant of calcite as a function of temperature and pressure. γ_{Ca}^{2+} is the calcium activity coefficient which is a function of ionic strength, temperature and pressure and is

determined by B-dot model and a_{Ca}^{2+} is the calcium ion activity. Kan et. al [15] suggested different scenarios for barite scale formation in wellbore based on different values of SI which can be summarized as follow:

A: If SI value is greater than 1.5 (at 120^0C) in the perforation zone at the bottom of well, precipitation occurs on the tubing walls and a large amount of crystals will form. In addition, it causes the SI value to decrease. Chemical inhibition at this stage is not efficient.

B: If SI value is between 0.3 and 1.5 in the perforation zone, scale formation occurs on the tubing walls at the bottom of well but the mass of barite scale per unit brine is negligible and thus is not a lasting problem.

C: If SI is less than 0.3 in the perforation zone, scale formation does not occur at the bottom of well and it may occur near the surface because of pressure and temperature change.

As it was mentioned, γ in Eq. 9 is the activity coefficient, which can be calculated based on B-dot model for the species as follows:

$$\text{Log } \gamma_i = -\frac{A_\gamma z_i^2 \sqrt{I}}{1+ a_i B_\gamma \sqrt{I}} + \text{BI} \quad (10)$$

where a_i is the ion size parameter, Aγ, Bγ and B are functions of temperature and I is the ionic strength calculated as follows:

$$I = \frac{1}{2}\sum_{k=1}^{n_{aq}} m_k z_k^2 \quad (11)$$

where z_k is the ionic charge of the k_{th} ion and m_k is the molality of the k_{th} ion.

2.4: Developed Models for Scaling Prediction

OSPMod was developed for prediction of scaling tendency based on the kinetic and thermodynamic data. By determining the critical saturation indices, this model first predicts the possibility of scale formation and then predicts the amount of scale formation in terms of scale profiles as a function of time and location [16]. This model, however, is limited to the well and surface locations. In other words, this model is not able to model scaling in reservoir.

AGIPS is a finite difference numerical model that was developed through coupling a chemical equilibrium code with a fluid flow simulator. This model is able to capture the impact of temperature and incompatible injection on the scaling issue in reservoir and wells. It also matched the results of experimental measurements on different water compositions taken from the North African oil fields [17].

FROCKI is another predictive model in which the impact of rock-fluid interactions on permeability impairment during production and injection in oil fields is investigated. In this model, the rock fluid interactions are related to the changes in temperature, ionic strength, pH and the hydro mechanical processes within reservoir [18].

2.5: Field Cases

Although the objective of water flooding operations is to increase the hydrocarbon recovery, in most cases the production because of water injection decreases dramatically after a short time if no scale inhibition action is taken. In this section, some real field cases of production decline because of scale formation are presented:

The first field case is Siri offshore oil field with four platforms which is located in Persian Gulf [19]. The oil field was discovered in 1970 and the drilling process started in 1975. A total number of 33 wells were drilled and 24 of them were chosen to be producer, seven were selected to be injectors and two to be producer/injector wells and production started in 1978. The total amount of cumulative oil production after the primary production was 13 MMSTB, which was about 2.3% of the oil in place. After the primary production, existence of appropriate conditions including an active aquifer leaded to operation of a waterflooding project in the oil field. With an objective of reservoir pressure maintenance and oil production increase, the water flooding process started in 1984 with an initial injection rate of 9100 bbl/day. However, after six years of injection and production, the water injection rate decreased to only 2200 bbl/day (7000 bbl/day reduction) as a result of scale formation and consequently the water flooding project was stopped. Figure 2- 3 shows the history of water injection in Siri oil field:

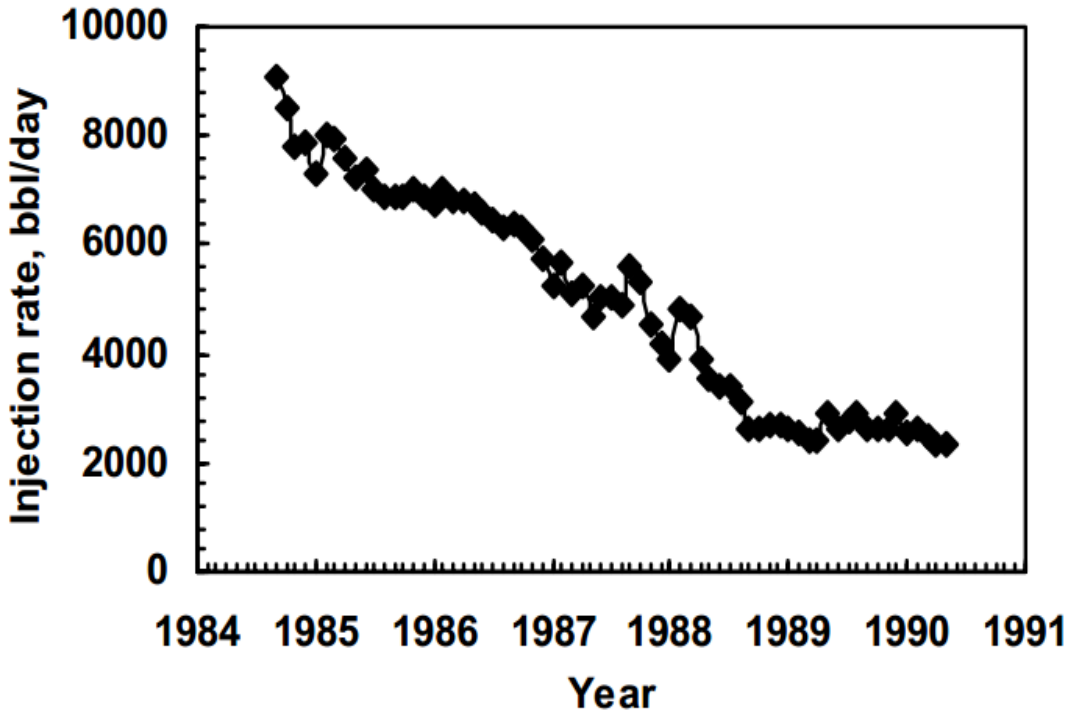

Figure 2- 3: Water injection rate of Siri oil field. After six years of injection, the water injection rate decreased from 9100 bbl/day to only 2200 bbl/day (7000 bbl/day reduction) as a result of scale formation [19].

Another severe case of oil field scale formation took place in a well in North Sea in Miller field. Oil production decreased from 30000 bbl/day to zero in 24 hours [20].

2.6: Permeability Impairment in Porous Media Resulting from Scale Formation

In the case of scale formation in porous media, the corresponding formation damage is evaluated in terms of permeability impairment. Models have been developed for predicting permeability reduction because of scaling issue with a mean absolute error of 11.16% compared with the experimental observations [12]. The detailed description of formation damage models have been reported in the literature [21]. Intelligent methods have been widely used in various fields of science and engineering [22-28]. In addition

to the analytical models, several researchers have attempted to employ intelligent models for studying scale formation [29, 30].

Extensive studies of scaling issue in the Iranian oil fields and production equipment resulted from incompatible water flooding projects have shown that the accuracy of results is mainly governed by the accuracy of the ions concentrations. The important parameters have been found to be pressure, the ions concentrations and the ratio of injected water to reservoir water. In addition, it has been demonstrated that the permeability reduction is larger at higher flow rates as more cations and anions react leading to larger saturation indices. Moreover, experimental works on the samples of the same filed have shown that permeability decreases up to 90% of the initial permeability depending on temperature, flow rate, injection period, initial permeability and the solution composition. In addition, it has been observed that the initial scale deposition rate is fast followed by a relatively slower ultimate deposition rate [1, 19, 31-34].

Formation damage has been studied in terms of a combination of mineral precipitation, clay swelling and fine migration in reservoirs as well. Multivariate numerical regression on experimental data has shown that by considering only the dominating chemical components, the impact of pore volume reduction on permeability impairment can be captured without including all the geochemical reactions involved in the process [35].

Studies on the impact of various ratios of injected water to formation water have shown that the largest permeability reduction occurs for the blends consisting of 90% formation water and 10% seawater. Moreover, it has been shown that more scales will

form when the injected seawater reaches the production wells and some studies have proposed that the permeability near the wellbore region can decrease up to 60% [11, 36].

2.7: Summary

The fundamentals of scale formation as well as the related literature were reviewed in this chapter. Various modeling and experimental approaches performed by the previous researchers were examined and a few field cases were presented.

A brief description of different types of scale including barium sulfate, calcium sulfate, strontium sulfate and calcium carbonate was provided. Some of the parameters that affect scale formation were found to be pressure, temperature, cumulative volume of injection fluid, the concentration of ions in the injected fluid, precipitation reaction rate and crystal growth rate, pore size distribution, fluid dynamics in porous media, porous media surface properties.

Chapter 3: Microscale Modeling of Mineral Deposition in Porous Media

Few studies have been carried out to study the impact of scaling issue on formation damage. Therefore, development of comprehensive models between the mechanisms of scaling tendency and porous media properties related to fluids conductivity and storativity is vital. In this chapter, a model based on multivariate regression analysis is developed for determining the permeability reduction in reservoir resulting from mineral scale deposition. To achieve this objective, 216 experimental data points covering a wide range of thermodynamic and reservoir conditions were collected from the literature [2]. Barium sulfate was considered as the main candidate of scale formation. The proposed model is considered to be a function of fluid pressure and reservoir temperature change, rate and time period of fluid injection, pore volume of the medium and solubility of $BaSO_4$. The statistical description of experimental data used in this study is illustrated in Table 3- 1.

Table 3- 1: Statistical description of the experimental dataset

Inputs/Outputs	Min	Max	Mean	SD
Injection rate, ft^3/min	$3.02*10^{-4}$	10^{-3}	$6.31*10^{-4}$	$1.87*10^{-4}$
Reservoir Temperature, °F	122	176	152	22.50
Fluid Pressure Gradient, psi	100	200	150	40.90
Time, min	10	120	65	34.60
Barite Solubility, ppm	137	1620	758	636
Pore Volume, ft^3	$3.98*10^{-4}$	$5.28*10^{-4}$	$4.66*10^{-4}$	$4.23*10^{-5}$
Kf/Ki	0.812	0.999	0.94	0.04

Additionally, various statistical and graphical analyses were employed to evaluate the accuracy and validity of the developed model. Moreover, Carman-Kozeny equation was incorporated into the model to find a modified model for porosity-permeability relationship in porous media when affected by scale formation.

3.1: Model Development- Multivariate Regression Analysis

In order to obtain an accurate predictive model, multivariate regression using least square error method was utilized [37-41]. The description of multivariate regression methodology is as follows:

It is assumed that the following relationship exists between the experimental data outputs and inputs

$$\vec{\mathbf{Y}} = \mathbf{A}\vec{\mathbf{X}} + \vec{\mathbf{e}} \tag{1}$$

Where, $\vec{\mathbf{Y}}$ represents the experimental outputs, $\vec{\mathbf{X}}$ represents the experimental input data, A is the coefficients of the proposed model and $\vec{\mathbf{e}}$ stands for the residuals between model predictions and the corresponding experimental values. This equation can be written in a more general matrix form as follows:

$$\begin{bmatrix} y_1 \\ y_2 \\ \vdots \\ y_{n1} \end{bmatrix} = \begin{bmatrix} x_{11} & x_{12} & \dots & x_{1k} \\ x_{21} & x_{22} & \dots & x_{2k} \\ \vdots & \ddots & \ddots & \vdots \\ x_{n1} & x_{n2} & \dots & x_{nk} \end{bmatrix} * \begin{bmatrix} a_1 \\ a_2 \\ \vdots \\ a_n \end{bmatrix} + \begin{bmatrix} e_1 \\ e_2 \\ \vdots \\ e_n \end{bmatrix} \tag{2}$$

Least square estimator defines the matrix of A in such a way that the summation of square residuals becomes as small as possible. This means that the following summation should be minimized:

$$\sum_{i=1}^{n} {e_i}^2 \quad (3)$$

which can be written in a matrix form as follows:

$$e'e = [e_1 \quad e_2 \cdots \quad e_n] \begin{bmatrix} e_1 \\ e_2 \\ \vdots \\ e_n \end{bmatrix} = \sum_{i=1}^{n} {e_i}^2 \quad (4)$$

Thus, in order to estimate the coefficient matrix A, the term ee' =(Y-XA)'(Y-XA) should be minimized which can be written as follows:

$$e'e = (Y - XA)'(Y - XA) \quad (5)$$

$$e'e = (Y' – A'X')(Y - XA) \quad (6)$$

$$e'e = YY' – A'X'Y – Y'XA+A'X'XA \quad (7)$$

Hence, the above expression should be minimized as written below:

$$\min [e'e = YY' – 2A'X'Y +A'X'XA] \quad (8)$$

In order to minimize the last equation, one is required to take a derivative with respect to A and equate it to zero. The following statement can be used for this purpose:

$$A'X'Y = (A'X'Y)' = Y'XA \quad (9)$$

then the derivation terms are as follow:

$$\frac{\partial(A'X'Y)}{\partial A} = X'Y \quad (10)$$

$$\frac{\partial(A'X'XA)}{\partial A} = 2X'XA \quad (11)$$

thus, the derivative of Eq. 7 becomes:

$$\frac{\partial(e'e)}{\partial A} = -2X'Y + 2X'XA = 0 \quad (12)$$

which leads to the following equation:

$$X'XA = X'Y \quad (13)$$

finally, A can be obtained by a simple manipulation as follows:

$$A = (X'X)^{-1}X'Y \quad (14)$$

This is the general formula for multivariate regression when there are many parameters (variables) affecting the output.

3.2: Evaluation of the Model Performance

3.2.1: Statistical Error Analysis

Several statistical parameters including Average Percentage Relative Error, Average Absolute Percentage Relative Error, Root Mean Square Error and Coefficient of Determination were utilized to measure the efficiency and accuracy of the proposed models [42, 43]. These parameters are defined as follow:

1. Average Percentage Relative Error (APRE). The relative deviation from the experimental data is calculated by this parameter and is defined based on the following equation:

$$E_r = \frac{1}{n}\sum_{i=1}^{n} E_i \quad (15)$$

Where E_i is Percentage Relative Error and is the relative deviation of a predicted value from the corresponding experimental value. It is defined based on the following equation:

$$E_i = \left[\frac{\left(\frac{\mathrm{Kf}}{\mathrm{Ki}} \right)_{\exp} - \left(\frac{\mathrm{Kf}}{\mathrm{Ki}} \right)_{\mathrm{rep./pred}}}{\frac{\mathrm{Kf}}{\mathrm{Ki}_{\exp}}} \right] \times 100 \Rightarrow i = 1,2,3,...,n \quad (16)$$

2. Average Absolute Percentage Relative Error (AAPRE). It is a measure of relative absolute deviation of the predicted values from the experimental data and is defined as follows:

$$E_a = \frac{1}{n} \sum_{i=1}^{n} | E_i | \quad (17)$$

3. Root Mean Square Error (RMSE): This parameter measures the data dispersion around zero deviation based on the following equation:

$$RMSE = \sqrt{\frac{1}{n} \sum_{i=1}^{n} \left(\frac{\mathrm{Kf}}{\mathrm{Ki}} i_{\exp} - \frac{\mathrm{Kf}}{\mathrm{Ki}} i_{\mathrm{rep./pred}} \right)^2} \quad (18)$$

4. Coefficient of Determination (R^2): This parameter is an indicator of how well the model predictions are close to the corresponding experimental values. The closer this value to unity, the better is the performance of the model in predicting experimental values. This parameter is calculated based on the following statement:

$$R^2 = 1 - \frac{\sum_{i=1}^{n}\left(\frac{\mathrm{Kf}}{\mathrm{Ki}} i_{\exp} - \frac{\mathrm{Kf}}{\mathrm{Ki}} i_{\text{rep./pred}}\right)^2}{\sum_{i=1}^{n}\left(\frac{\mathrm{Kf}}{\mathrm{Ki}} i_{\text{rep./pred}} - \overline{\frac{\mathrm{Kf}}{\mathrm{Ki}}}\right)^2} \quad (19)$$

where $(\overline{\frac{\mathrm{Kf}}{\mathrm{Ki}}})$ is the experimental data mean.

3.2.2: Graphical Error Analysis

In order to get a better vision of the performance of the developed models, graphical error analyses were employed. These methods are defined as follow:

1. Crossplot: In this technique, the experimental data points are plotted versus the predicted values by the model. The closer the relationship of these points to the unit slope line, the more accurate is the model.

2. Error Distribution: In order to investigate the possible error trend of the model, this technique measures data scatter around the zero error line.

3.3: Model Validation and Results

As it was mentioned earlier, barium sulfate was considered as the main source of scale formation in porous media resulted from incompatible water injection based on the following reaction:

$$Ba^{2+} + SO_4^{2-} \Leftrightarrow BaSO_4 \quad (20)$$

Since the scaling behavior highly depends on the concentration of Ba^{2+} in the formation water, two different conditions including high barium concentration (2200 ppm) and

normal Ba^{2+} concentration (250 ppm) were considered and two models were developed at these conditions. The reason for choosing two models for these specific concentrations was the availability of experimental data at these two conditions. However, if more experimental values are available, a more general model considering the effect of barium concentration might be developed to combine the models at different concentrations.

As mentioned earlier, several parameters affect scale precipitation and deposition in petroleum reservoirs. In this work, the most important parameters based on the experimental data were considered to have direct effect on permeability reduction resulting from formation of mineral crystals. Temperature has a direct effect on dissolution reaction rate and causes an increase in barium sulfate dissolution when it is increased. This situation does not favor scale deposition and thus, permeability decline tends to decrease when temperature increases. Another important parameter affecting scaling tendency is the injected pore volume. Precipitation rate differs from the case in which fluid is moving fast over a small surface area during a specific time period to the case in which fluid velocity is controlled by a large surface area. Therefore, the following functionality was considered to exist between permeability reduction and the aforementioned parameters in which the power values were found empirically:

$$\frac{K_f}{K_i} \sim (T^{\frac{1}{6}}, PV_{inj}^{\frac{1}{4}}) \tag{21}$$

Another important group affecting scaling behavior was found to be a combination of pressure, salt solubility and available pore volume of the medium. Pressure has an effect on the solubility product of the salt and also affects the dynamic of deposition.

Solubility of the mineral plays a significant role in the scaling tendency of the mixed fluids and can be found in the literature at different conditions [44]. Finally, the available pore volume of the medium has a close relationship with the amount of volume available for solid deposition, as it can be an indicator of the reactive surface area of the mineral. The following relationship was found to exit between the mentioned group and corresponding permeability impairment:

$$\frac{K_f}{K_i} \sim \text{Ln}\,(\Delta P.V_P.S_{BaSO4}) \qquad (22)$$

Hence, after analyzing the experimental data and performing statistical analysis, the following model was developed for prediction of permeability reduction in porous media as a result of barium sulfate scale formation at high barium concentration:

$$\exp\left(\frac{K_f}{K_i}\right) = A_0 + A_1T^{1/6} + A_2(Qt)^{1/4} + A_3\text{Ln}\,(V_P) + A_4\text{Ln}\,(S_{BaSO4}) + A_5\text{Ln}\,(\Delta P) \qquad (23)$$

In this equation, K_f/K_i is the permeability damage ratio (K_f and K_i are the final and initial permeability, respectively), Q is the injection rate in ft^3/min, t is the injection time in min, V_P is the pore volume of the porous media in ft^3, S_{BaSO4} is the solubility of $BaSO_4$ in ppm and ΔP is the pressure difference in psi. A_1, A_2, A_3, A_4, and A_5 are empirical coefficients and A_0 is the model intercept that were calculated by using multivariate regression analysis. These values are reported in Table 3- 2.

At normal concentration of barium (250 ppm), a similar model with different constants was developed in which the units for the input variables are the same as the previous model and the constants are shown in the same table.

Table 3- 2: Model Constants at high Barium concentration (2200 ppm) and normal Barium concentration (250 ppm)

Constant	High Barium concentration (2200 ppm)	Normal barium concentration (250 ppm)
$\mathbf{A_0}$	-1.69×10^{2}	-1.33×10^{1}
$\mathbf{A_1}$	1.14	7.89×10^{-1}
$\mathbf{A_2}$	-1.51	-7.61×10^{-2}
$\mathbf{A_3}$	1.69×10^{2}	6.06
$\mathbf{A_4}$	-1.04×10^{-1}	-5.45×10^{-1}
$\mathbf{A_5}$	1.09×10^{-1}	9.40×10^{-2}

In order to evaluate the performance of the proposed models, various statistical analyses including Average Percentage Relative Error (APRE), Average Absolute Percentage Relative Error (AAPRE), Root Mean Square Error (RMSE) and Coefficient of Determination (R^2) were performed. The results are summarized in Table 3- 3. As can be observed from this table, for the case of high barium concentration, the values of AAPRE, APRE, RMSE and R^2 are 0.803, -0.011, 0.024 and 0.945, respectively. In addition, these values for the case of normal barium concentration were found to be 0.411, -0.003, 0.014 and 0.937, respectively. These results confirm the superiority of the proposed model in predicting permeability alteration caused by barium sulfate scale formation in reservoir porous media with high accuracy and validity.

Table 3- 3: Statistical parameters of permeability reduction models using 208 data points

Barium Concentration	$\mathbf{E_a}$ (%)	$\mathbf{E_r}$ (%)	RMSE	$\mathbf{R^2}$
High Concentration of Barium	0.889	-0.021	0.102	0.948
Normal Concentration of Barium	0.427	-0.005	0.056	0.941

In the next step, crossplots of the models were plotted to demonstrate the performance of the models in predicting the experimental values. Figure 3- 1 shows the crossplot of the high barium concentration model. As can be observed, the data points lie on the unit slope line with a R^2 of 0.948 which demonstrates the high accuracy of the model in estimating the experimental data points.

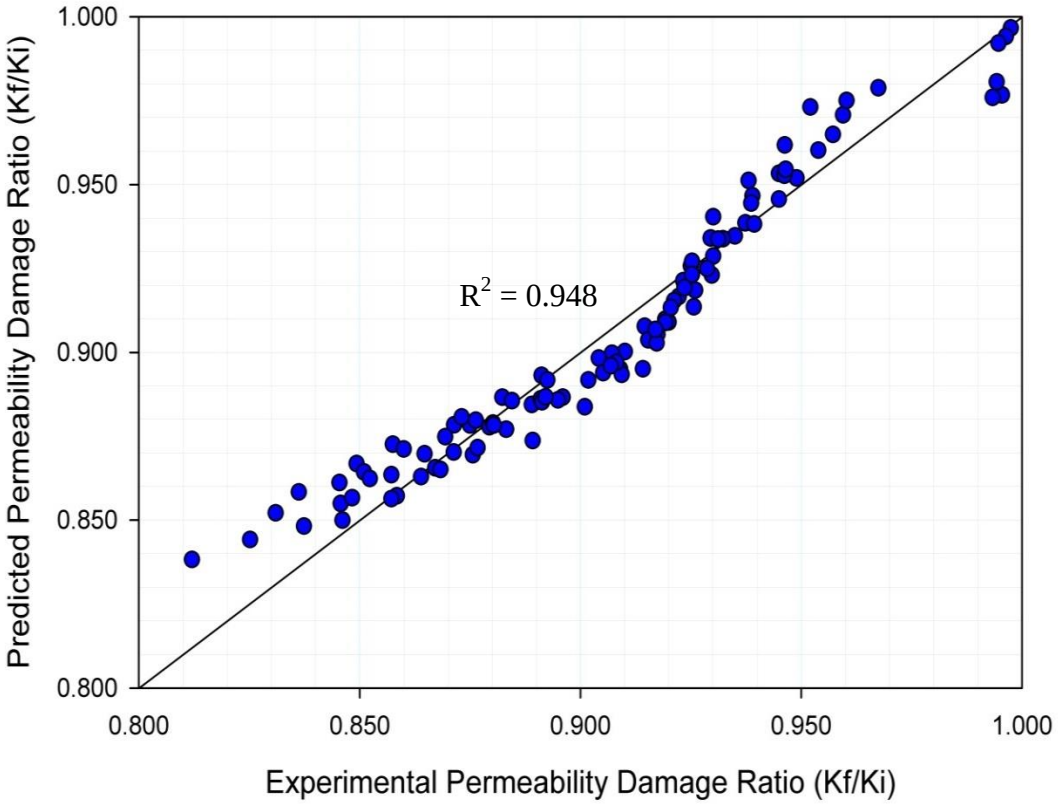

Figure 3- 1: Crossplot of the proposed model for permeability ratio at high barium concentration.

Figure 3- 2 illustrates the crossplot of normal barium concentration model. Similarly, as shown in this figure, the data points lie on the unit slop line with a R^2 value of 0.941,

which again verifies the robustness of the proposed model in estimating damage ratio when barium has a normal concentration in the solution.

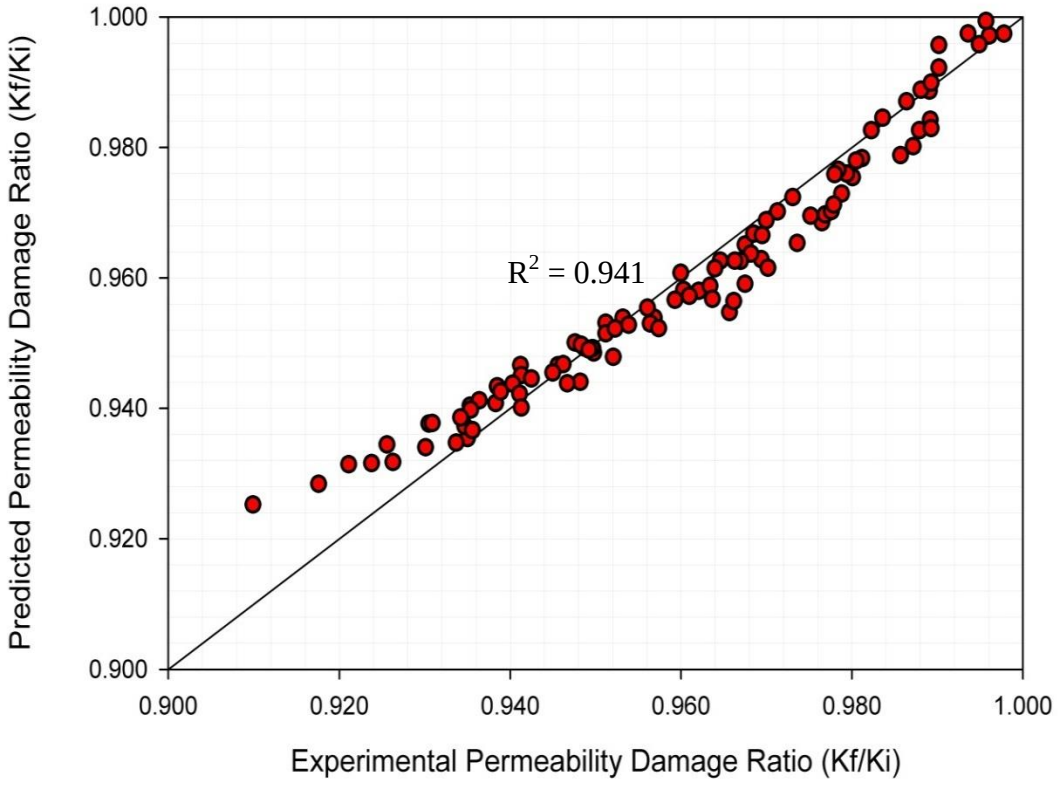

Figure 3- 2: Crossplot of the proposed model for permeability ratio at normal barium concentration.

In addition, error distribution curves for both models were plotted to get a better vision of the error trend of the models when the experimental values tend to increase. Figure 3-3 shows the error distribution curve of the first model. As can be seen, the cloud of data points is located around the zero error line, which indicates the good performance of the model in matching with the experimental values. Also, it can be concluded from this figure that the proposed model does not have an error trend when the experimental damage ratio increases.

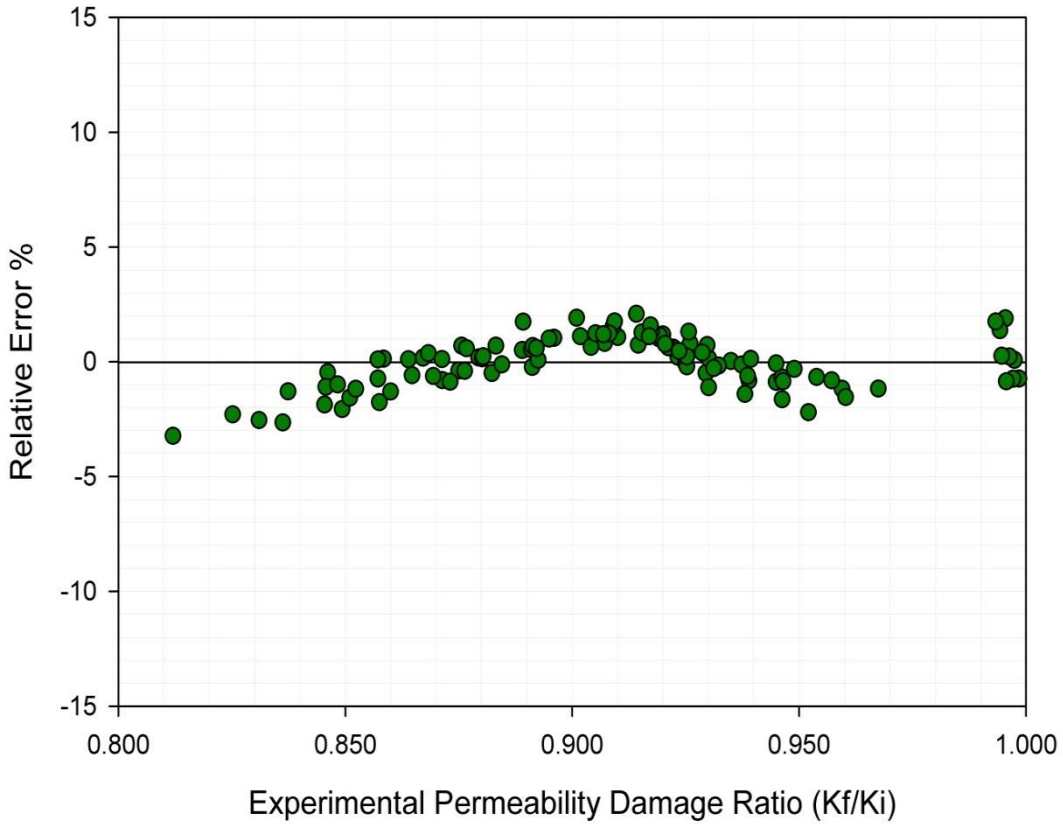

Figure 3- 3: Error distribution plot of the model at high barium concentration. The cloud of data points is located around the zero error line indicating that the proposed model for high barium solution does not have an error trend.

Figure 3- 4 shows the error distribution curve of the second model. Similarly, this figure demonstrates that the second model is able to predict the experimental values with high accuracy and without a significant error trend.

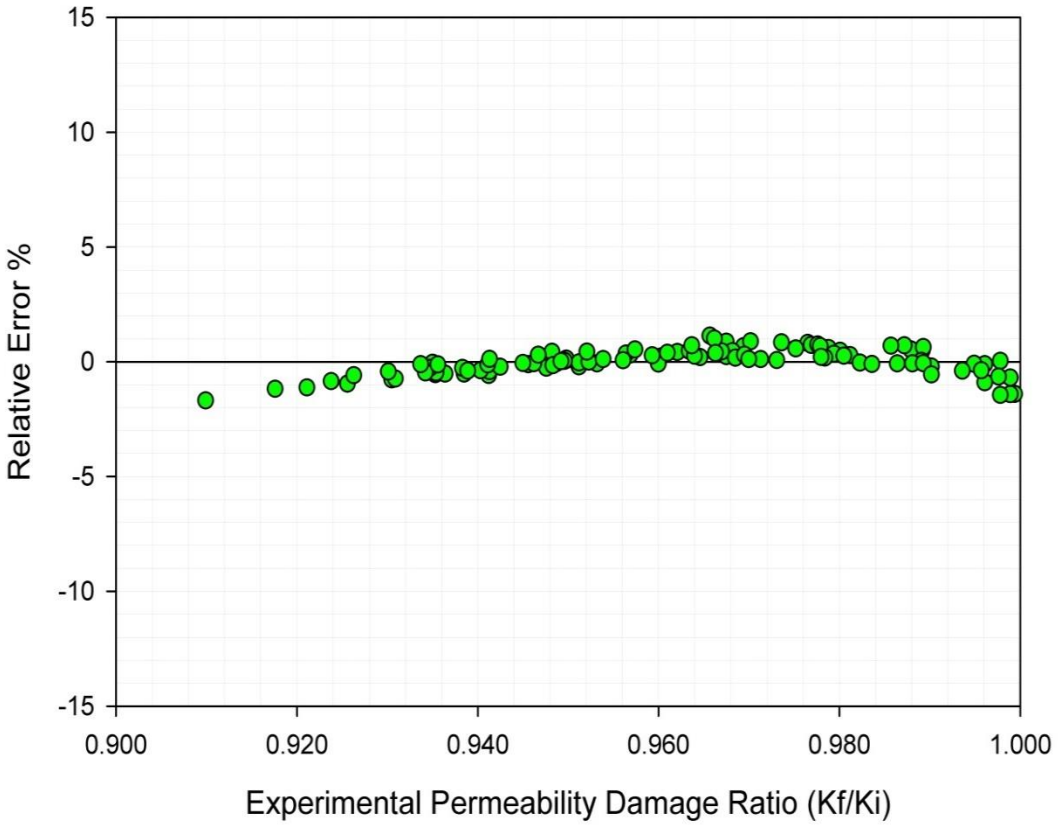

Figure 3- 4: Error distribution plot of the model at normal barium concentration. The cloud of data points is located around the zero error line indicating that the proposed model for normal barium solution does not have an error trend.

Additionally, relevancy factor [45] was utilized to investigate the impact of each input parameter on permeability impairment. A larger absolute value of relevancy factor (r) between an input and output means the greater impact of that input on the output. Relevancy factor is defined based on the following equation:

$$r\left(inp_k, (\frac{k_f}{k_i})_i\right) = \frac{\sum_{i=1}^{n}\left(inp_{k,i} - inp_{k,ave}\right)\left((\frac{k_f}{k_i})_i - (\frac{k_f}{k_i})_{ave}\right)}{\sqrt{\sum_{i=1}^{n}\left(inp_{k,i} - inp_{k,ave}\right)^2 \sum_{i=1}^{n}\left((\frac{k_f}{k_i})_i - (\frac{k_f}{k_i})_{ave}\right)^2}} \quad (24)$$

In this equation $(\frac{K_f}{K_i})_i$ and $(\frac{K_f}{K_i})_{ave}$ denote the i^{th} and average values of predicted permeability ratio, respectively. k denotes the input variables (injected fluid volume, temperature, pressure gradient, barite solubility and pore volume of the medium). $inp_{k,i}$ represents the i^{th} value of the k^{th} input and $inp_{k,avg}$ is the average value of the k^{th} input. The results of relevancy factor analysis are depicted in Figure 3- 5. As it was mentioned earlier, if an input variable displays a larger r value, it has a greater effect on the output when other parameters remain constant. As can be seen in Figure 3- 5, the injected pore volume has the greatest impact on permeability reduction. This is because a larger amount of solid crystals can be deposited and consequently, a larger portion of the pores and throats are plugged. Barite solubility has the next greatest impact on permeability reduction as more solid particles with larger reactive surface area cause more precipitation and hence more pore volume reduction. Temperature and pore volume of the medium have less impacts on permeability reduction than the mentioned parameters and pressure gradient has the smallest impact on permeability reduction resulting from barite scale formation.

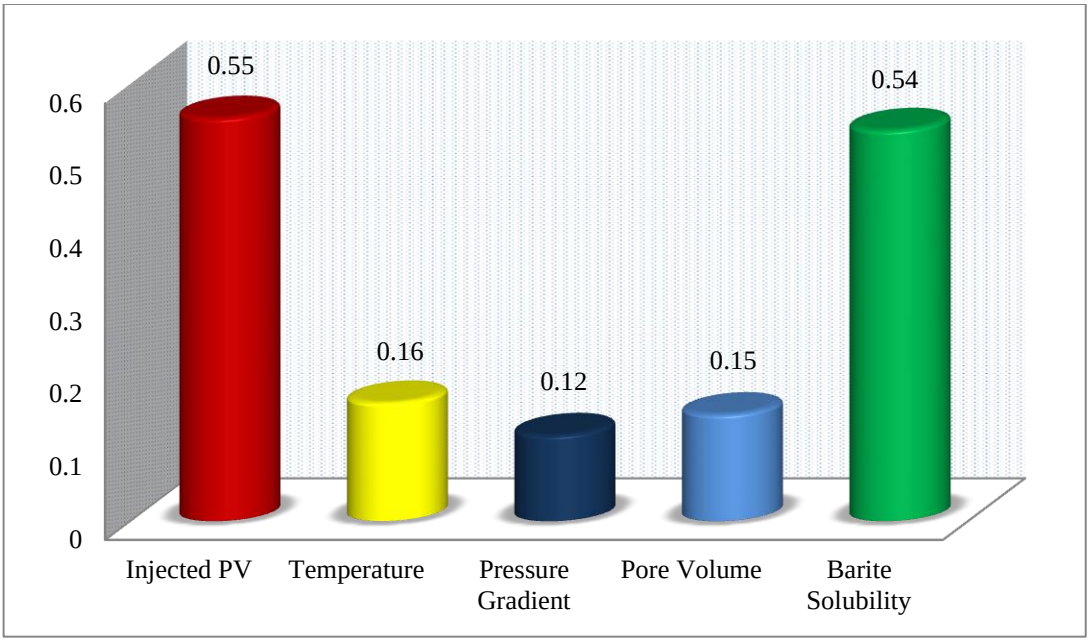

Figure 3- 5: Relative impact of input parameters on permeability reduction. The injected pore volume has the largest impact on scale formation followed by barite solubility. Pressure has a smaller impact on scaling compared to the other parameters

3.4: Modified Carman-Kozeny Model

In order to model the permeability-porosity relationship in porous media, Carman-Kozeny assumed that porous media is made of a bundle of tubes as shown in Figure 3-6.

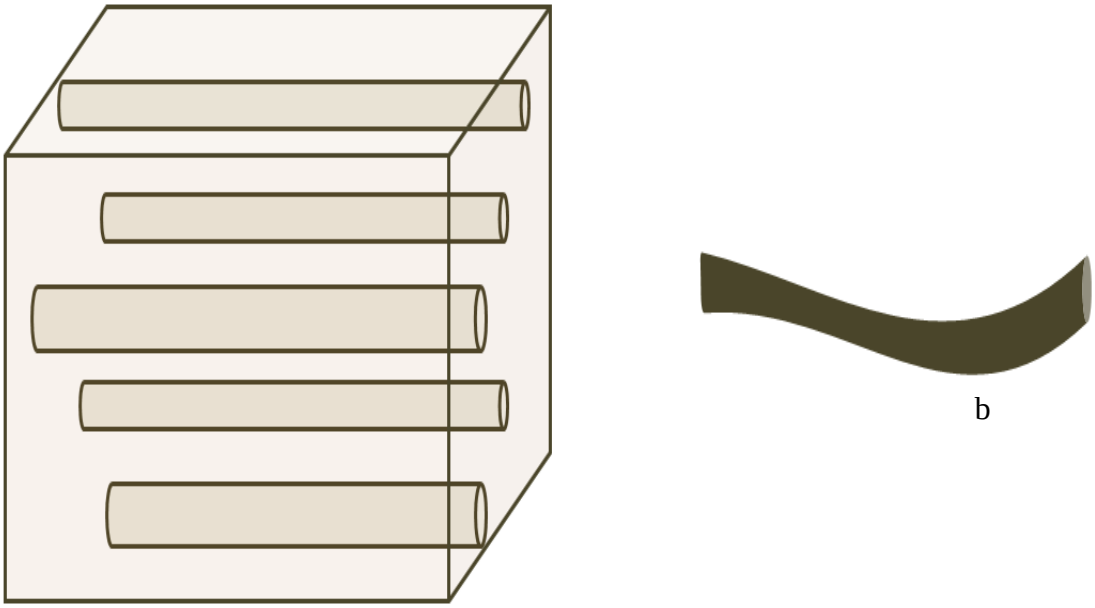

a b

Figure 3- 6: a: Ideal capillary tubes. b: An actual tube with tortuosity

Based on Poiseuille's equation for laminar flow in a tube, fluid pressure gradient in flow direction can be defined as follows [46-48]:

$$\frac{dp}{dx} = -\frac{32\mu u l'}{l\phi D^2} \tag{25}$$

Where D is the diameter of the tube, ϕ is the porosity of medium, μ is the viscosity of fluid, u is the fluid velocity, l' is the true length of the tube and l is the layer length, all in SI units. Usually, $\frac{l'}{l}$ is called tortuosity as shown in Figure 3- 6.b. Assuming that the pore volume is Q, Solid volume is Q_s and porosity is ϕ, the following relationship exists in a porous material:

$$Q = \frac{\phi Q_s}{(1-\phi)} \tag{26}$$

Assuming that the pore space is made of tubes with diameter D and solid space is made of uniform spheres with diameter D_s, the above equation ends up with the following equation for the pore space diameter:

$$D = \frac{2\phi D_S}{3(1-\phi)} \tag{27}$$

Substituting this equation into Poiseuille's Equation leads to the following equation:

$$\frac{dp}{dx} = - \frac{72\mu u l'(1-\phi)^2}{l D_s \phi^3} \tag{28}$$

The Darcy's law is defined as the following equation:

$$q = \frac{K}{\mu} A \frac{\Delta P}{L} \tag{29}$$

Thus, the following equation for permeability is obtained which is called Carman-Kozeny relationship:

$$k = \frac{1}{72\tau} \frac{\phi^3 D_s^2}{(1-\phi)^2} \tag{30}$$

Now recall the developed models for permeability reduction resulting from scale formation at high barium concentration:

$$\exp\left(\frac{K_f}{K_i}\right) = A_0 + A_1 T^{1/6} + A_2 (Qt)^{1/4} + A_3 \mathrm{Ln}\,(VP) + A_4 \mathrm{Ln}\,(S_{BaSO4}) + A_5 \mathrm{Ln}\,(\Delta P) \tag{31}$$

This equation can be simplified to the following equations:

$$\exp\left(\frac{K_f}{K_i}\right) = A_0 + A_1 T^{1/6} + A_2 (Qt)^{1/4} + \text{Ln}\left(VP^{A3} S_{BaSO4}{}^{A4} \Delta P^{A5}\right) \quad (32)$$

By taking a natural log from both sides, the damage ratio K_f/K_i can be found as the following statement:

$$\frac{K_f}{K_i} = \text{Ln}\left[A_0 + A_1 T^{1/6} + A_2 (Qt)^{1/4} + \text{Ln}\left(VP^{A3} S_{BaSO4}{}^{A4} \Delta P^{A5}\right)\right] \quad (33)$$

As discussed earlier, Carman-Kozeny equation gives the following equation for permeability-porosity relationship:

$$k = \frac{1}{72\tau} \frac{\phi^3 D_s^2}{(1-\phi)^2} \quad (34)$$

Attempting to find porosity as a function of permeability from this equation, the following equation is obtained by using MATLAB software package:

$$\phi = \frac{C}{3} + M - \frac{N}{M} \quad (35)$$

In which:

$$C = \frac{72\Gamma K}{D_S^2} \quad (36)$$

$$M = \left(\frac{C}{2} + \left(N^2 + \left(\frac{C^3}{27} - \frac{C^2}{3} + \frac{C}{2}\right)^2\right)^{1/2} - \frac{C^2}{3} + \frac{C^3}{27}\right)^{1/3} \quad (37)$$

$$N = \frac{6C - C^2}{9} \quad (38)$$

Finally, the damaged porosity ratio as a result of barium sulfate scale formation in porous media is obtained based on the following equation:

$$\frac{\phi_f}{\phi_i} = \frac{C'}{3} + M' - \frac{N'}{M'} \tag{39}$$

In which:

$$C' = \frac{72\Gamma\frac{Kf}{Ki}}{D_s^2} \tag{40}$$

$$M' = \left(\frac{\frac{72\Gamma\frac{Kf}{Ki}}{D_s^2}}{2} + \left(N^2 + \left(\frac{\left(\frac{72\Gamma\frac{Kf}{Ki}}{D_s^2}\right)^{\wedge}3}{27} - \frac{\left(\frac{72\Gamma\frac{Kf}{Ki}}{D_s^2}\right)^{\wedge}2}{3} + \frac{\left(\frac{72\Gamma\frac{Kf}{Ki}}{D_s^2}\right)}{2}\right)^2\right)^{1/2} - \frac{\left(\frac{72\Gamma\frac{Kf}{Ki}}{D_s^2}\right)^{\wedge}2}{3} + \frac{\left(\frac{72\Gamma\frac{Kf}{Ki}}{D_s^2}\right)^{\wedge}3}{27}\right)^{1/3} \tag{41}$$

$$N' = \frac{6\frac{72\Gamma\frac{Kf}{Ki}}{D_s^2} - \left(\frac{72\Gamma\frac{Kf}{Ki}}{D_s^2}\right)^{\wedge}2}{9} \tag{42}$$

And

$$\frac{K_f}{K_i} = \text{Ln}\left[A_0 + A_1 T^{1/6} + A_2 (Qt)^{1/4} + \text{Ln}\left(VP^{A3} S_{BaSO4}{}^{A4} \Delta P^{A5}\right)\right] \tag{43}$$

Eq. 39 is the general form of porosity reduction based on permeability damage ratio resulting from barium sulfate scale formation when incompatible water is injected into the reservoir.

3.5: Sensitivity Analysis

In this part of the study, the results of sensitivity analysis based on the scale precipitation thickness are presented.

Let us assume that the pore volume of porous medium is made of n uniform tubes with radius r and length l' and the bulk volume has a length of l as shown in Figure 3- 7.

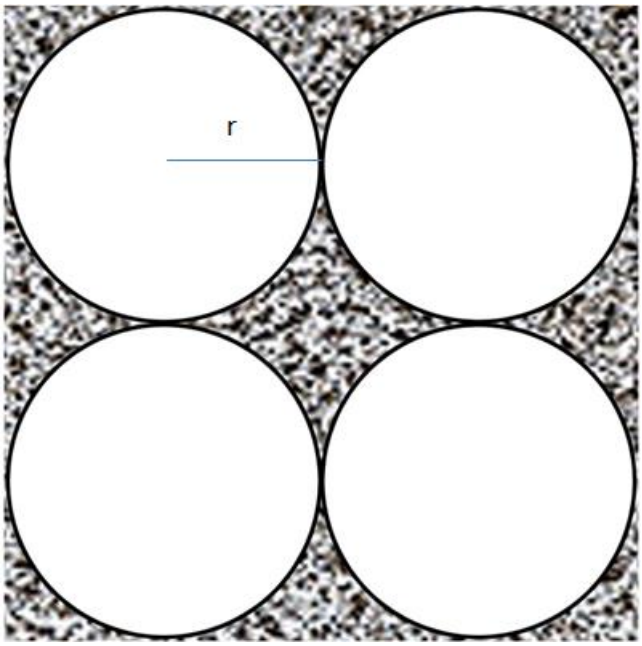

Figure 3- 7: Porous medium with cylindrical tubes. There are n uniform tubes with radius r and length l' and the bulk volume has a length of l.

If there are n cylindrical tubes in the medium, the corresponding porosity is calculated based on the following equation:

$$\phi_1 = \frac{n\pi r^2 l'}{BV} \tag{44}$$

In this equation, BV stands for bulk volume. Now assuming that scale formation has occurred as shown in Figure 3- 8, we will have reduction in porosity because of the pore size reduction.

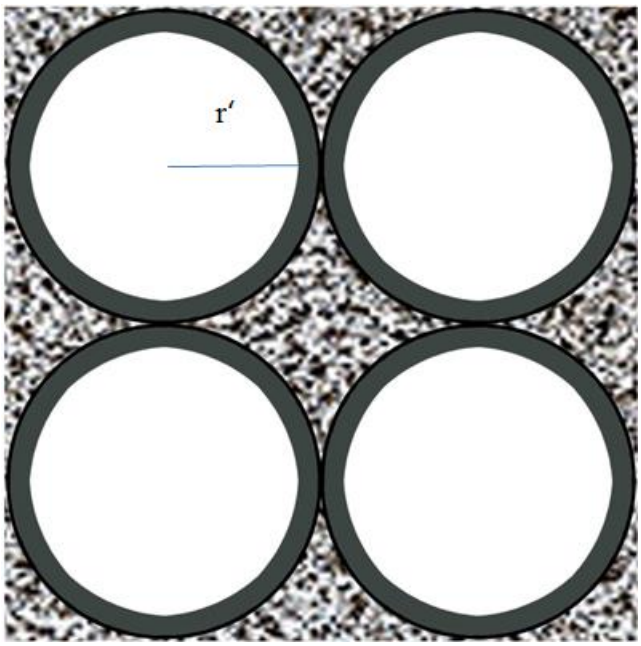

Figure 3- 8: Porous medium with cylindrical tubes after scale formation. Porosity decreases as the pore sizes become smaller becaasue of scale formation. It is assumed that the pores are uniformly plugged.

In this case, the corresponding porosity is calculated based on the new radius of the tubes, r', based on the following equation:

$$\phi_2 = \frac{n\pi r'^2 l'}{BV} \tag{45}$$

Now let us assume that the following relationship exists between the old radius, r, and the new radius, r':

$$\frac{r'}{r} = x \tag{46}$$

Where, x can get any values between zero and one depending on the severity of scale formation.

Therefore, the corresponding porosity ratio is calculated based on the following statement:

$$\frac{\phi_2}{\phi_1} = \frac{\frac{n\pi r'^2 l'}{BV}}{\frac{n\pi r^2 l'}{BV}} = \frac{r'^2}{r^2} = X^2 \quad (47)$$

Thus, the porosity ratio is proportional to the radius ratio squared.

It is worth noting that the same conclusion is drawn when a general type of pore volume consisting of cylindrical tubes with different radii is considered as shown in Figure 3- 9.

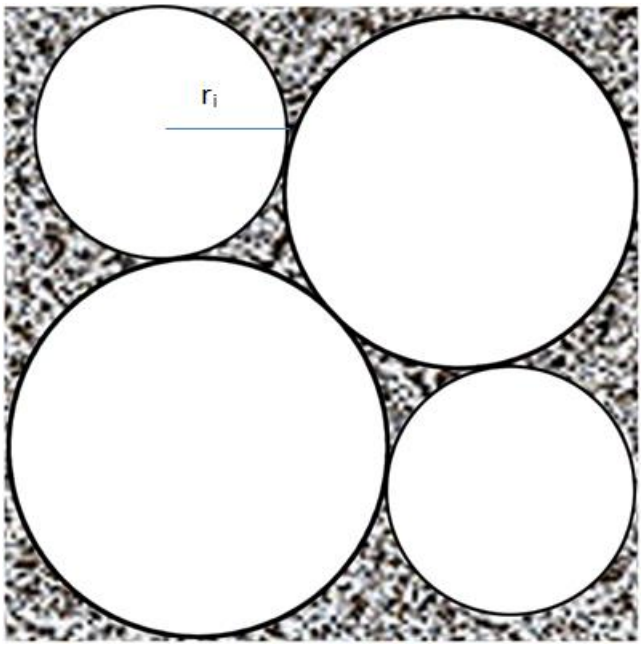

Figure 3- 9: Porous medium with nonuniform pore size distribution. Porosity reduction resulted from scale formation will be the same as the case in which the pore size distribution is uniform

In this case, porosity values before and after scale precipitation when the pore radius reduction ratio is the same can be obtained based on the following statements:

$$\phi_1 = \frac{\sum_{i=1}^{n}(\pi r_i^2 l')}{BV} \quad (48)$$

$$\phi_2 = \frac{\sum_{i=1}^{n}(\pi r'_i{}^2 l')}{BV} \tag{49}$$

$$\frac{\phi_2}{\phi_1} = \frac{\frac{\sum_{i=1}^{n}(\pi r'_i{}^2 l')}{BV}}{\frac{\sum_{i=1}^{n}(\pi r_i{}^2 l')}{BV}} = \frac{\sum_{i=1}^{n}(x r_i)^2}{\sum_{i=1}^{n} r_i{}^2} = x^2 \tag{50}$$

This is the same observation obtained in the case of identical tubes.

In the next step, in order to investigate the effect of pore size reduction on permeability ratio, we need to combine the above derivations with the Carman-Kozeny equation based on the following steps:

Let us assume two cases for Carman-Kozeny equation as before scale formation shown by K_1 and after scale formation shown by K_2. We have:

$$K_1 = \frac{1}{72\tau}\frac{\phi_1^{\,3} D_s^2}{(1-\phi_1)^2} \tag{51}$$

$$K_2 = \frac{1}{72\tau}\frac{\phi_2^{\,3} D_s^2}{(1-\phi_2)^2} \tag{52}$$

Assuming that the solid diameter and tortuosity remain the same, we have:

$$\frac{K_2}{K_1} = \frac{\frac{\phi_2^{\,3}}{(1-\phi_2)^2}}{\frac{\phi_1^{\,3}}{(1-\phi_1)^2}} \tag{53}$$

Based on Eq. 50 we can substitute ϕ_2 with $\phi_1 x^2$ to get the following statement:

$$\frac{K_2}{K_1} = x^6\left(\frac{1-\phi_1}{1-\phi_1 x^2}\right)^2 \quad (54)$$

Based on the severity of damage, different values for pore size reduction ranging from 0.9 to 0.1 can be assumed. Therefore, sensitivity analysis based on the radius reduction can be performed. The results of sensitivity analysis are illustrated in Figure 3- 10. As can be seen in this figure, permeability ratio decreases significantly when the thickness of precipitation increases. In addition, this figure states that when the thickness of scale precipitation is large, permeability reduction occurs more significantly compared with the case that pore volume reduction is not significant. Different values of porosity were considered for a better vision of the permeability behavior.

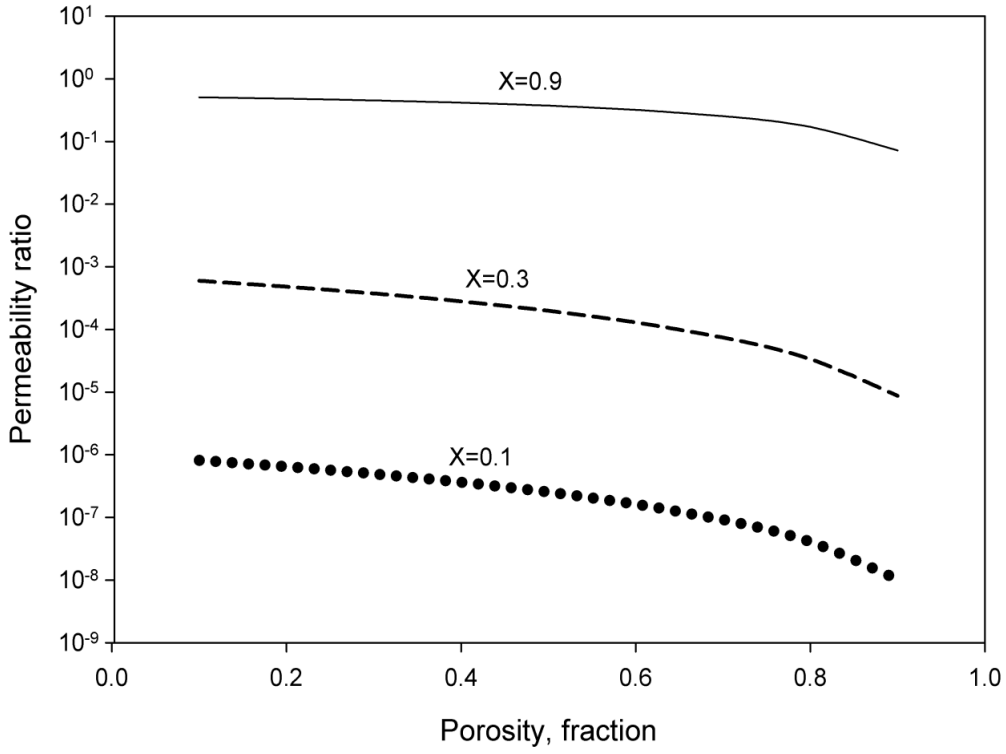

Figure 3- 10: permeability ratio decreases significantly when the thickness of precipitation increases

3.6: Summary

In this chapter, Multivariate Regression Analysis technique was employed to develop two models for estimating permeability reduction caused by barium sulfate scale formation during water flooding. To achieve this objective, 216 data sets covering a wide range of reservoir and thermodynamic conditions were collected from the literature. The main parameters affecting formation damage because of scale deposition were considered to be the injected fluid volume, pressure gradient of the fluid, reservoir temperature, solubility of barium and the available pore space. The results of statistical and graphical analysis showed that the models are able to predict formation damage

with high accuracy and promising performance. Moreover, the models were incorporated into Carman-Kozeny equation to obtain a dynamic third order equation for porosity alteration as a function of permeability reduction.

Chapter 4: Macro scale Modeling of Scale Formation in Reservoir and its Impact on Reservoir Performance

4.1: Mechanism of Barite Precipitation

Bethke [49, 50] proposed the following expression for mineral precipitation (or dissolution) rate:

$$r_\beta = A_\beta k_\beta \left(1- \frac{Q_\beta}{K_{eq,\beta}}\right) \quad \beta = 1,\ldots, R_{mn} \tag{1}$$

in Eqn. 4 , k_β is the rate constant, A_β is the reactive surface area of mineral β, $K_{eq,\beta}$ is the chemical equilibrium constant which can be found as a function of temperature in the literature [51, 52] and r_β is the reaction rate, all in SI units. The term $\frac{Q\beta}{Keq,\beta}$ in Eqn. 4 is the saturation index of the reaction. If the saturation index is less than unity, mineral precipitation occurs. When the saturation index is one, the reaction is at equilibrium.

Q_β is the activity product for mineral β and can be determined by the following equation:

$$Q_\beta = \prod_{k=1}^{n_{aq}} a_k^{v_{k\beta}} \tag{2}$$

where, a_k is the activity of component k and $v_{k\beta}$ is the stoichiometry coefficient. The following expression shows the relationship between the activity of and molality of components:

$$a_i = \gamma_i m_i \qquad i=1,\ldots, n_{aq} \tag{3}$$

in Eqn. 6, m_i is the molality of component i and γ_i is the activity coefficient which can be calculated based on B-dot model as follows:

$$\text{Log } \gamma i = -\frac{A_y z_i^2 \sqrt{I}}{1+ \dot{a}_i B_y \sqrt{I}} + BI \quad (4)$$

where $\dot{a}_i$ is the ion size parameter, Aγ, Bγ and B are functions of temperature and I is the ionic strength calculated as follows:

$$I = \frac{1}{2}\sum_{k=1}^{n_{aq}} m_k z_k^2 \quad (5)$$

where z_k is the ionic charge of the k_{th} ion.

As it was mentioned earlier, A_β is the reactive surface area of mineral β. It is known that in high porosity sandstones, the accessible fraction of reactive minerals is around one third while this value can be as small as one fifth for shaly sandstones [53]. The following mole change based equation is used for calculating the reactive surface area:

$$A_\beta = A_\beta^0 \frac{N_\beta}{N_\beta^0} \quad (6)$$

where A_β is the reactive surface area of mineral β at current time, A_β^0 is the reactive surface area at time zero, N_β is the moles of mineral β per unit grid block volume at current time and N_β^0 is defined at time zero.

The following expression is used to calculate the change in porosity resulting from mineral dissolution/precipitation:

$$\hat{\phi} = \phi^* - \sum_{\beta=1}^{n_m} \left(\frac{N_\beta}{p_\beta} - \frac{N_\beta^0}{p_\beta}\right) \quad (7)$$

where, $\hat{\phi}$ is the reference porosity when dissolution/precipitation is included, ϕ^* is the reference porosity without mineral dissolution/precipitation and p is the molar density of mineral β.

Here, we examine the above equations by giving an example describing the mechanisms of barite precipitation used in the simulations. The parameters are chosen the same as the literature values used for the simulations. The reservoir formation water used in this research is considered rich in barium cation. The injected seawater is considered rich in sulfate anion. The molalities of barium and sulfate were used from real formation and sea waters in literature [50] to be 0.0043 m and 0.028 m, respectively. Barium and sulfate react with each other to form barite based on the following reaction:

$$Ba^{2+} + SO_4^{2-} \rightarrow BaSO_4 \quad (8)$$

Depending on the activity product and equilibrium constant of the above reaction, different scenarios i.e., precipitation and/or dissolution can happen. The activity product is defined as follows:

$$Q = \prod_{i=1}^{n_{aq}} a_i^{\nu_i} \quad (9)$$

In fact, activity product is the ratio of the multiplication of products (barite) to the reactants (barium and sulfate) powered by their stoichiometry coefficients. Based on Eq. 28, the activity product of the barite reaction is calculated as follows:

$$Q = \frac{a_{BaSO_4}}{a_{Ba^{2+}} a_{SO_4^{2-}}} \quad (10)$$

The activity of minerals is usually assumed one while the activity of the ions are calculated using their activity coefficients based on the following equation:

$$a_i = \gamma_i m_i \tag{11}$$

where m is the molality of the ions and γ is the activity coefficient of the ions. A simple formula for calculating the activity coefficients is obtained by using the Debye–Hückel theory based on the following expression:

$$Log\,\gamma_i = -Az_i^2\sqrt{I} \tag{12}$$

where z is the charge of the ions, A is a constant (usually 0.5092) and I is the Ionic strength of ions calculated based on the following formula:

$$I = \frac{1}{2}\sum m_i (z_i)^2 \tag{13}$$

As it was mentioned before, the activity of barite is assumed one. The activities of barium and sulfate are calculated using Eq. 31-33 as follows:

$$I = \frac{1}{2}\sum m_i (z_i)^2 = \frac{1}{2}[0.0043\times 2^2 + 0.028\times 2^2] = 0.065$$

$$Log\,\gamma_{Ba^{2+}} = -Az_{Ba}^2\sqrt{I} = 0.5092\times 2^2\times\sqrt{0.065} = 0.52 \Rightarrow \gamma_{Ba^{2+}} = 10^{0.52} = 3.29$$

$$Log\,\gamma_{SO_4^{2-}} = -Az_{SO_4^{2-}}^2\sqrt{I} = 0.5092\times 2^2\times\sqrt{0.065} = 0.52 \Rightarrow \gamma_{SO_4^{2-}} = 10^{0.52} = 3.29$$

$$a_{Ba^{2+}} = \gamma_{Ba^{2+}} m_{Ba^{2+}} = 3.29\times 0.0043 = 0.01$$

$$a_{SO_4^{2-}} = \gamma_{SO_4^{2-}} m_{SO_4^{2-}} = 3.29\times 0.028 = 0.09$$

Therefore, the activity product of barite precipitation becomes:

$$Q = \frac{a_{BaSO_4}}{a_{Ba^{2+}} a_{SO_4^{2-}}} = \frac{1}{0.01 \times 0.09} = 1111.11$$

Equilibrium constant of a reaction is defined based on the following equation:

$$\ln K_{eq} = -\Delta G_r^0 / RT \tag{14}$$

where ΔG_r^0 is the Gibbs free energy of the reaction at standard condition and is reported for different species in literature usually in kJ/mol, R is the gas constant and T is the temperature in K. This equation is used for calculating the equilibrium constant at standard condition (298.15 K). A similar equation is derived for determining the equilibrium constant at different temperatures based on the following equation:

$$\ln K_{eq,T} = \ln K_{eq,298.15} - \frac{\Delta H_r^0}{R}\left(\frac{1}{T} - \frac{1}{298.15}\right) \tag{15}$$

In the above equation, ΔH_r^0 is the enthalpy of the reaction in kJ/mol which is also reported in the literature for different species.

In order to calculate the equilibrium constant of barite at the reservoir temperature in this study, 161^{0}F (344.817K), first the values of ΔG_f^0 and ΔH_f^0 of the species should be found from the literature. These values are reported in Table 4- 1.

Table 4- 1: The thermodynamic properties of barium, sulfate and barite [54]

Property \ Component	Ba^{2+}	SO_4^{2-}	$BaSO_4$
ΔG_f^0 (kJ/mol)	-560.74	-744.63	-1362.186
ΔH_f^0 (kJ/mol)	-537.64	-909.27	-1473.19

ΔG_r^0 and ΔH_r^0 of the reaction is calculated by subtracting the ΔG_f^0 and ΔH_f^0 of the reactants from the products multiplied by their stoichiometry coefficients.

Based on Eq. 28, these values for barite precipitation become:

$$\Delta G_r^0 = \Delta G^0_{BaSo_4} - \Delta G^0_{Ba^{2+}} - \Delta G^0_{SO_4^{2-}} = -1362.186 - (-560.74) - (-744.63) = \text{-56.82 kJ/mol}$$
$$\Delta H_r^0 = \Delta H^0_{BaSo_4} - \Delta H^0_{Ba^{2+}} - \Delta H^0_{SO_4^{2-}} = -1473.19 - (-537.64) - (-909.27) = \text{-26.28 kJ/mol}$$

Therefore, the equilibrium constant of barite precipitation at standard condition becomes:

$$\ln K_{eq} = -\Delta G_r^0 / RT = -\frac{\text{-56.82} \times 10^3}{8.314 \times 298.15} = 22.92 \text{ (dimensionless)}$$

By a simple manipulation, the log of equilibrium constant can be obtained as follows:

$$\log K_{eq} = \frac{\ln K_{eq}}{2.303} = \frac{22.92}{2.303} = 9.95$$

This value could be directly read from a table in literature [55] as it was previously read in the previous sections. Depending on how the reaction is defined (on what side barite is and on what side barium and sulfate are), this value could have a negative sign.

However, since the activity product will also be reverse, the ratio of these two values known as the saturation ratio will represent the same result.

For calculating ΔG_r^0 at the reservoir temperature, Eq. 35 is used as follows:

$$\ln K_{eq,T} = \ln K_{eq,298.15} - \frac{\Delta H_r^0}{R}\left(\frac{1}{T} - \frac{1}{298.15}\right) = 22.92 - \frac{-26.28\times10^3}{8.314}\left(\frac{1}{344.817} - \frac{1}{298.15}\right) = 21.48$$

$$\Rightarrow K_{eq,T} = \exp(21.48) = 2131304350$$

If the saturation index is less than one, which is the case here, it means that the solution is far from equilibrium and the activity product should increase to get closer to the equilibrium constant to approach equilibrium. Based on the reaction that we have defined in Eq. 28, for increasing the activity product, barite should precipitate. In other words, the reaction will proceed to the right and barite will precipitate. This is confirmed by the results of the numerical simulation illustrated in the following sections.

4.2: Reservoir Base Case Model

The reservoir properties used in in this study are summarized in Table 4- 2. The reservoir fluid components and compositions are shown in Table 4- 3.

Table 4- 2: Reservoir properties

Grid	30*30*1
Grid block sizes	$\Delta x = 20$ ft $\Delta y = 20$ ft $\Delta z = 150$ ft
Permeability in all directions	300 mD
Porosity	0.2
Depth of reservoir top	9500 ft
Reservoir temperature	161 ^{0}F
Initial reservoir pressure	4800 psi at 9600 ft
Rock compressibility	$3*10^{-6}$

Table 4- 3: Hydrocarbon components and compositions

CO_2	0.0023
N_2	0.0063
CH_4	0.3624
C_2H_6	0.0279
C_3H_8	0.0225
C_4H_{10}	0.0204
C_5H_{12}	0.0139
C_6H_{14}	0.0166
C_{7+}	0.5277

Barium sulfate was considered to be the precipitating mineral in the reservoir as a result of incompatible water injection. The concentration of barium in the formation water and

the composition of sulfate in the seawater were used from bethke [50]. The mineral precipitation reaction properties were used from [55, 56]. These properties are all shown in Table 4- 4. The relative permeability curves are shown in Figure 4- 1.

Table 4- 4: Chemical reaction properties

Barium molality in formation aqueous phase	0.0043 m
Sulfate molality in seawater	0.028 m
Activation energy of barite precipitation reaction	22 kJ/mol
Barite reactive surface area	900 m^2 / m^3 of bulk volume of mineral
log of barite Reaction rate constant at 25^0C	-8 mol/m^2s
Log of barite chemical equilibrium constant	-9.97

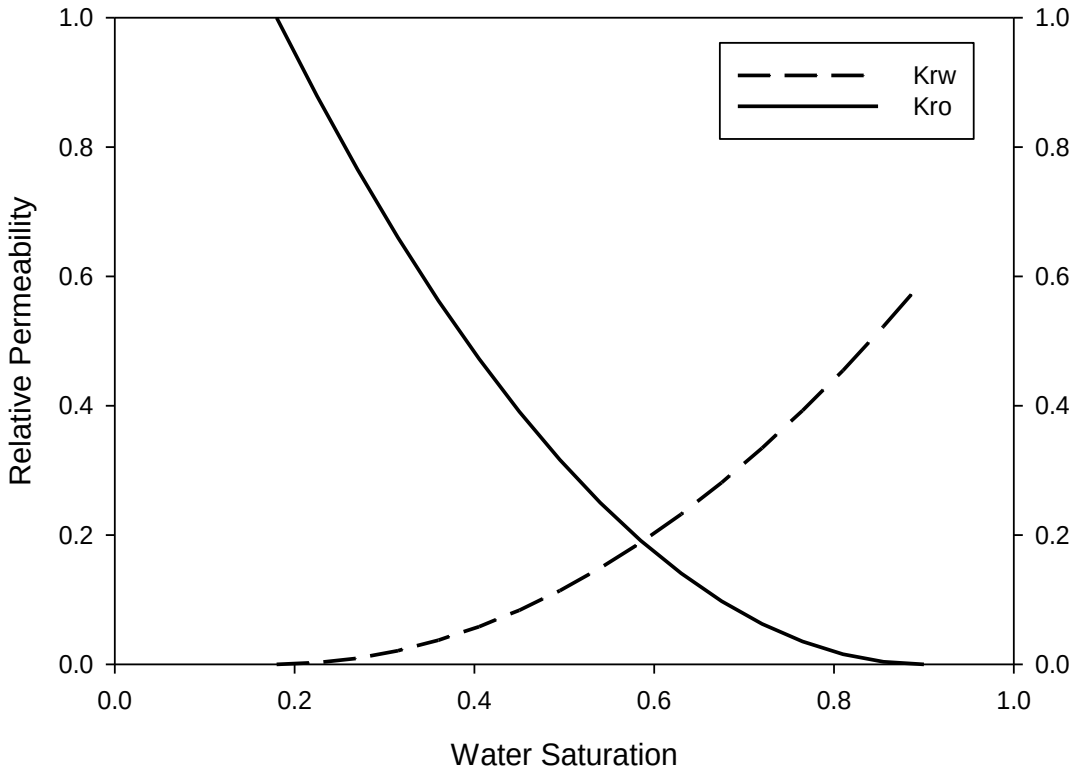

Figure 4- 1: The relative permeability curves of water and oil

Two wells were considered to be actively injecting and producing at the corners of the reservoir as shown in Figure 4- 2 and production was continued for nine years. The minimum bottom hole pressure for the production well was set to 2500 psi. Also, this well was constrained to a maximum surface liquid rate of 300bbl/day. The injection well was constrained to a maximum water rate of 340 bbl/day and subjected to a large maximum bottom hole pressure to ensure a constant injection rate.

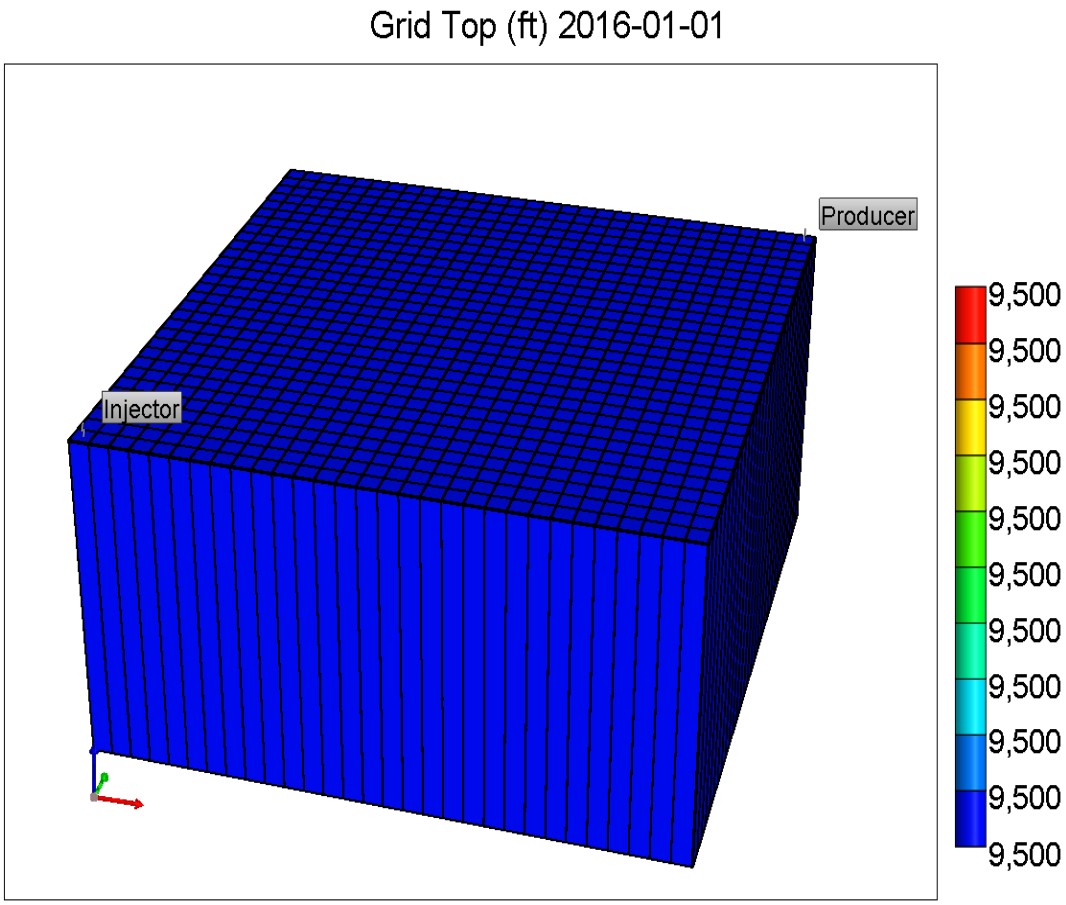

Figure 4- 2: Reservoir geometry

4.3: Simulation of a Synthetic Oil Field Affected by Scale Formation

In order to investigate the impact of mineral scale deposition on reservoir performance, barium sulfate was considered to be the scaling mineral occurring in the reservoir during water flooding. Investigation the impact of multiple minerals including barium sulfate and calcium sulfate will be the focus of the future sections.

Figure 4- 3, Figure 4- 4 and Figure 4- 5 illustrate the amounts of barium, sulfate, barite and the corresponding porosity reduction after three, six and nine years of incompatible

water flooding, respectively. As it was mentioned earlier, barium sulfate precipitates based on the following reaction:

$$Ba^{2+} + SO_4^{2-} \rightarrow BaSO_4 \quad (16)$$

The stoichiometry coefficients of barium and sulfate are equal and as the concentration of barium in the formation water is lower than that of sulfate in the seawater (Table 3), barium is consumed and some sulfate ions will remain in the aqueous phase. Also, barite mineral which was set to be zero initially, will form and increase by continuing the injection as verified by Figure 4- 3, Figure 4- 4 and Figure 4- 5. As can be observed in these figures, the locations of porosity reduction in the reservoir are directly related to the mineral deposition of barite within the reservoir. In other words, wherever barite scaling occurs, porosity reduction is observed. Also, it can be noted that the porosity reduction wave is propagated in a radial manner from the injection well towards the production well. Also, as can be seen in some of the grid blocks porosity drops down from 0.2 to nearly 0.08 which significantly affects the reservoir performance.

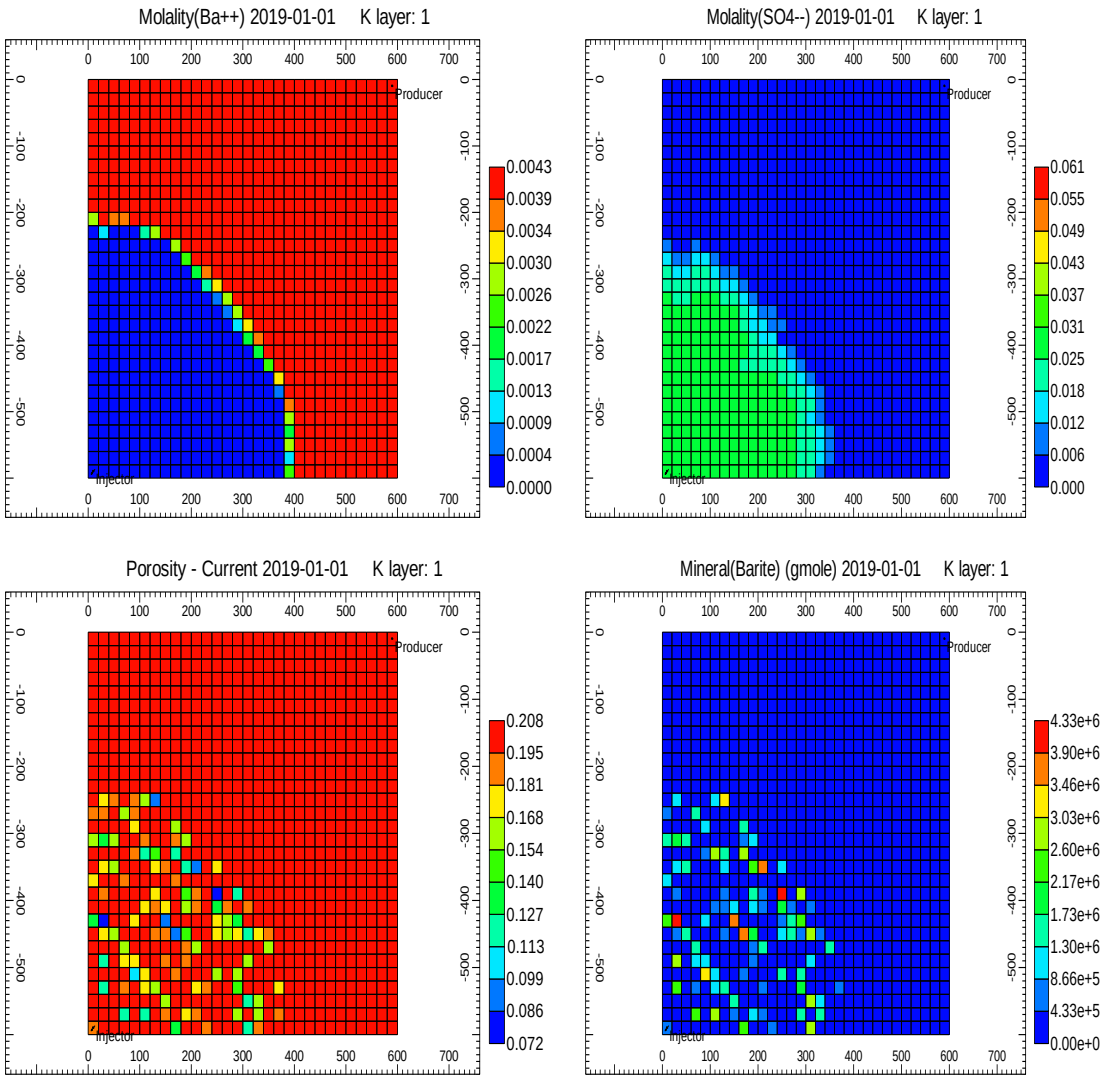

Figure 4- 3: Location and amounts of barium, sulfate, barite and porosity after three years of flooding

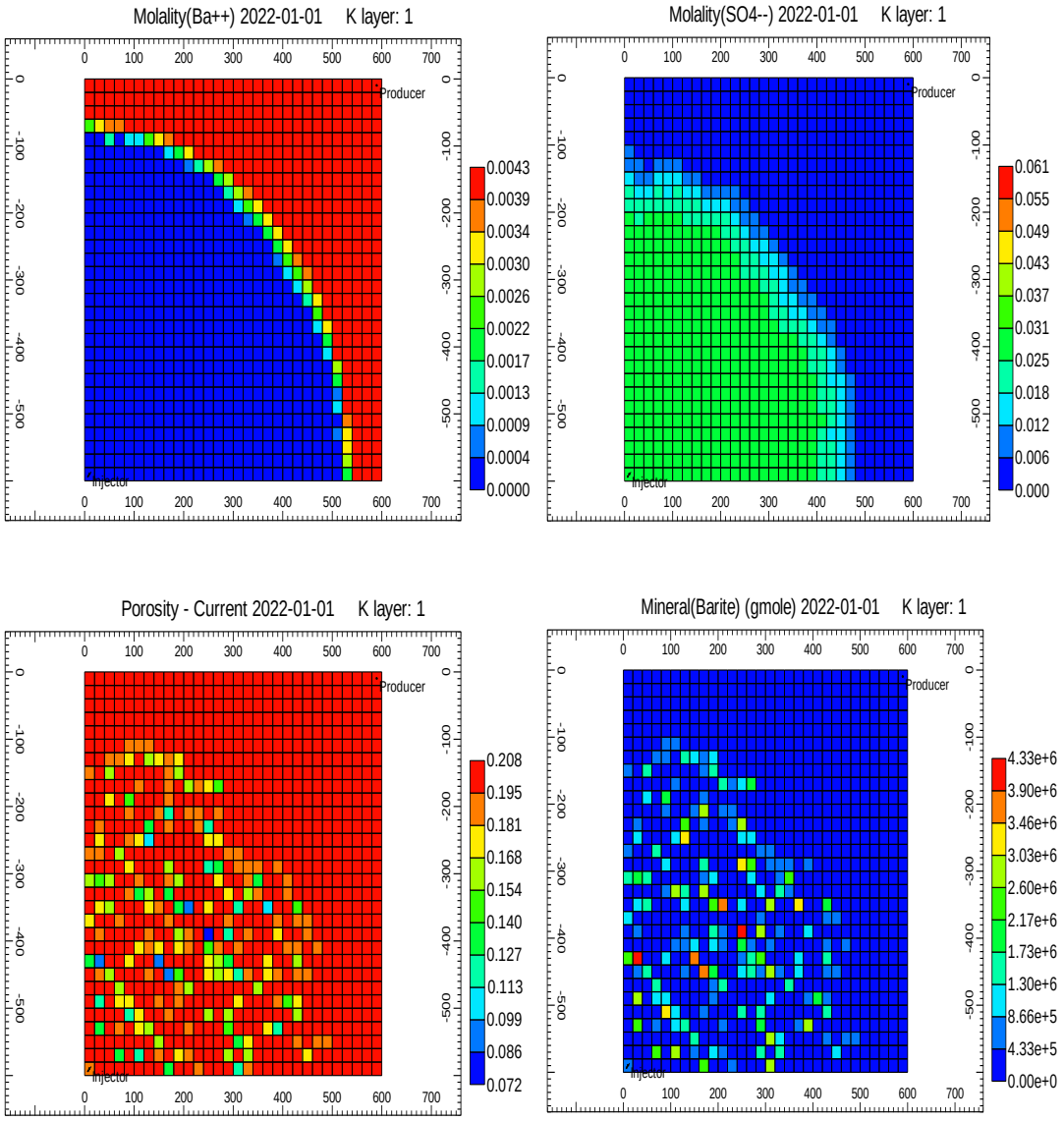

Figure 4- 4: Location and amounts of barium, sulfate, barite and porosity after six years of flooding

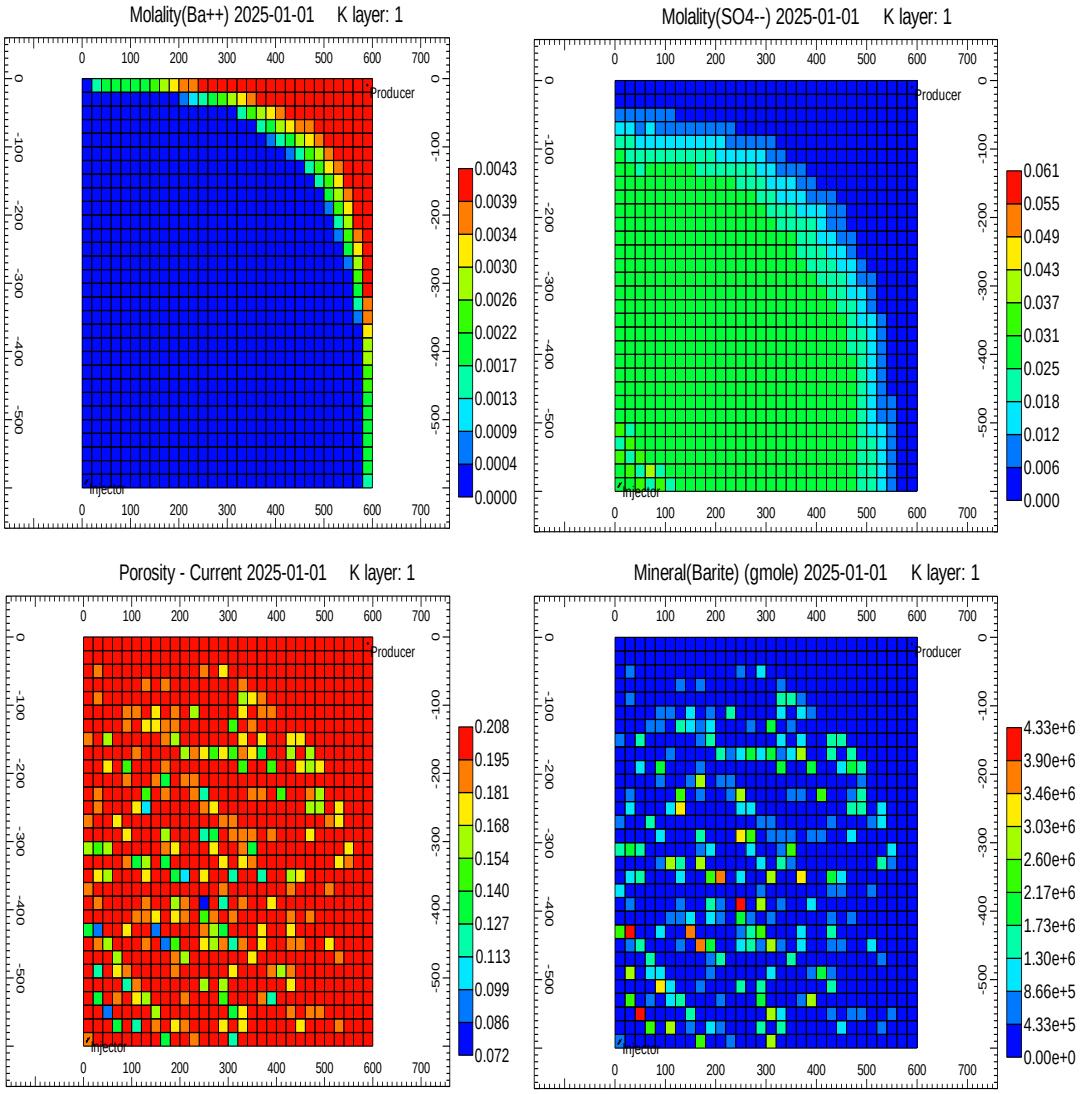

Figure 4- 5: Location and amounts of barium, sulfate, barite and porosity after nine years of flooding

4.4: Impact of Scale Formation on Injection Performance

4.4.1: Impact of Barite Scale Formation on Injection Bottom Hole Pressure

In this section, the impact of scale formation in reservoir on well performance is investigated. A one dimensional reservoir with the same properties discussed before

was considered. In the first scenario, the injection well was assigned to a large maximum bottom hole pressure to ensure a constant water injection of 340 bbl/day. The production well was constrained to a minimum bottom hole pressure of 2500 psi and a maximum liquid rate of 300 bbl/day. Water flooding was continued for nine years without including the geochemical reactions and the resulting scale formation. In the second scenario, the chemical reactions were included while other parameters were kept the same. The results are illustrated in Figure 4- 6. As can be observed, when the scaling issue is not considered in the flooding process, the required bottom hole pressure for the injection well increases from 4800 psi (initial reservoir pressure) to 5542 psi to keep the constant injection rate. In the second case, however, this pressure increases up to 10246 psi which is around 5000 psi increment in the injection pressure. These results are in close agreement with the real oil field experience in Siri offshore oil field in Persian Gulf [19] where the water flooding project was stopped after six years as the water injection rate decreased from 9100 to 2200 bbl/day as a result of scaling issue. Here, we ensured a constant injection rate to determine the bottom hole pressure needed for this operation. These results suggest that care should be taken while water flooding projects are designed. Ignoring the scaling issue and impacts of mineral deposition in the reservoir will significantly affect the outcome of water injection process.

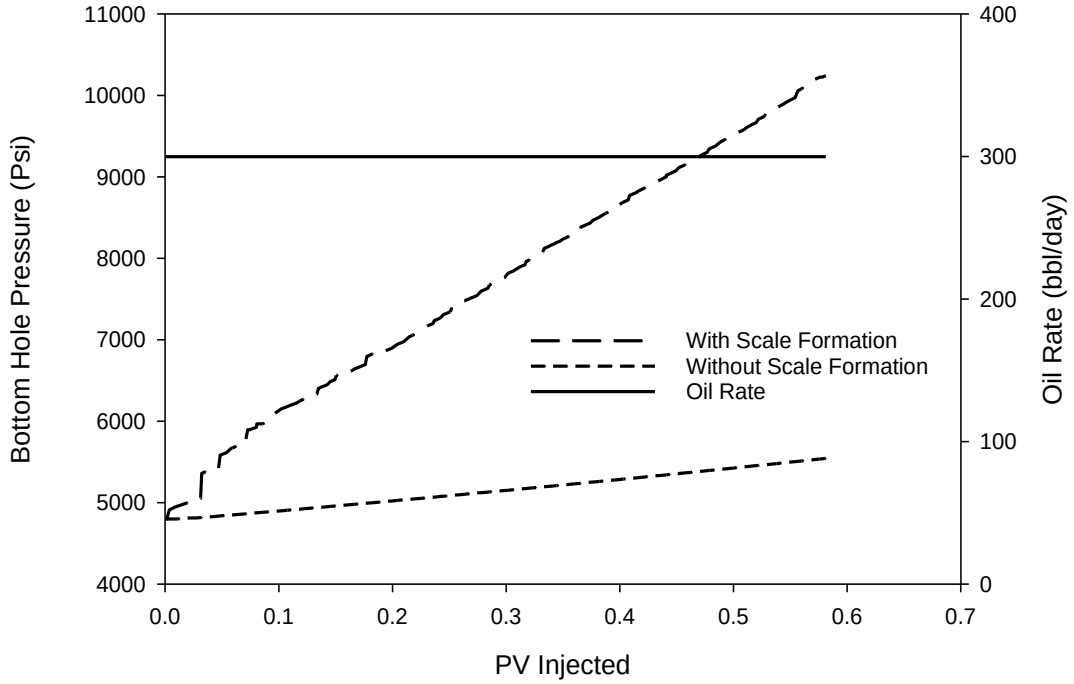

Figure 4- 6: The impact of scaling on well performance. Scaling leads in an increase in the bottom hole pressure required for a constant production rate.

4.4.2: Sensitivity Analysis Based on Reactive Surface area of Barite

Dissolution and precipitation rates are affected by the reactive surface area of minerals. One simple model for determining the dissolution/precipitation rate is as follows [57]:

$$r = Ak(1-\Omega) \tag{17}$$

where r is the dissolution/precipitation rate in mol/s, A is the reactive surface area of the mineral in m^2, k is the rate constant in mol/m^2s and Ω is the saturation index.

The reactive surface area of minerals has been a question of interest among the researchers [57, 58]. In numerical simulations, A is usually normalized and reported in m^2/m^3 of bulk volume of rock. When the reaction is far from equilibrium (dissolution

and precipitation conditions), the rate is essentially dependent on the reactive surface area and pH. In fact, the variation in reactive surface area affect the reactive transport properties within a rock [57]. In addition, it has been found that the reactive surface area changes as the reaction proceeds.

Reactive surface area of minerals depends on their grain size. Different methods are used to measure the reactive surface area of minerals such as atomic force microscopy, vertical scanning interferometry and laser confocal microscopy. However, these experimental approaches [58] provide limited information for reactive transport modeling as the surface area is highly affected by the scale at which the process is observed. In a geological carbon sequestration study, Shu et al. [58] showed that reactive surface has a significant impact on mineralization trapping of CO_2 in saline aquifers. They studied seven cases including different sizes for grain diameters of calcite and anorthite, which leads in different reactive surface areas for these minerals. They concluded that because of a reduction in the surface areas of calcite and anorthite, the amount of dissolved anorthite and the amount of precipitated calcite and kaolinite decrease significantly. They also concluded that during 500 years, mineral trapping of CO_2 decreases from 11.8% to 0.65% because of the reduction in the reactive surface areas of calcite and anorthite from 838 to 83.8 m^2/m^3.

Here, in order to investigate the effect of amount of precipitation on well performance, a sensitivity analysis based on the reactive surface area of barite was studied. The inputs are the same as discussed in the previous section and the results are shown in Figure 4-7. As can be observed, an increase in the reactive surface area of barite leads in an increase in the required injection bottom hole pressure for maintaining the constant

production rate. In addition, it can be observed that by increasing the amount of precipitation, the injection curves deviate from a smooth trend

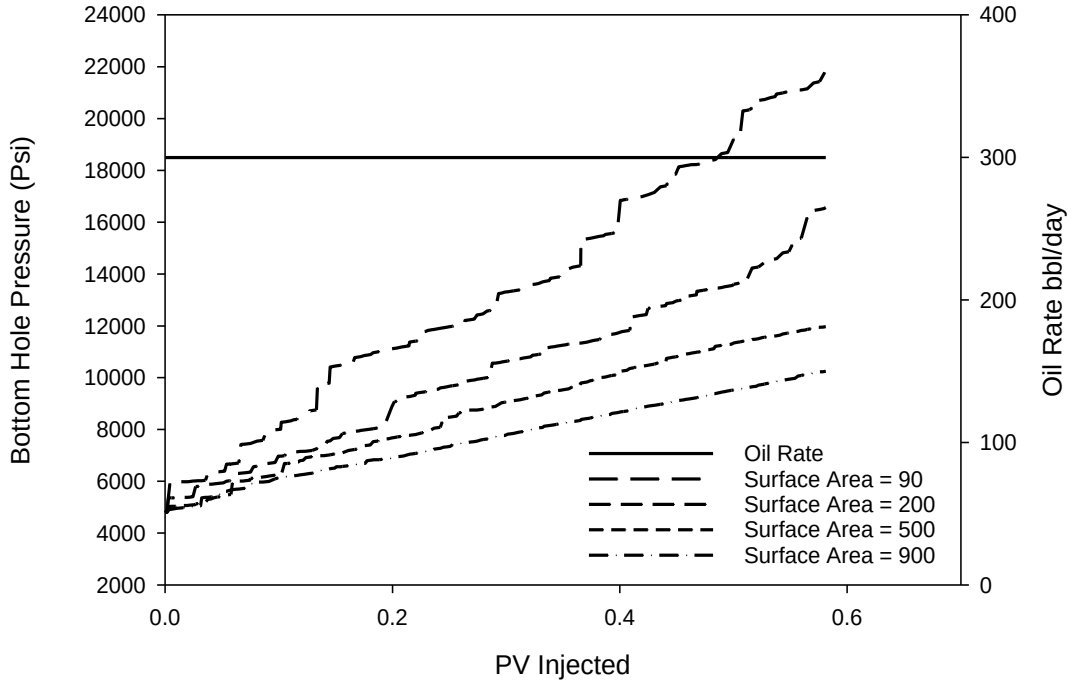

Figure 4- 7: Impact of precipitation amount on well performance. Reactive surface area has a direct relationship with the amount of precipitation and a larger surface area leads in a higher bottom hole pressure required for injection.

4.5: Impact of Scale Formation on Recovery Factor

In this section, the impact of scale formation on oil recovery is investigated. The salinity of the injected water was increased to correctly capture the effect of scale precipitation on oil recovery. In addition, the production well was allowed to produce based on the rate and pressure increase in the injection well with a minimum bottom hole pressure of 3200 psi. The injection well was constrained to a maximum bottom hole pressure of 3355 psi and a maximum water rate of 300 bbl/day. Again, two scenarios were

considered: one without considering scale formation and one with including the impact of scaling issue. The results for the first case are illustrated in Figure 4- 8. As can be observed, water flooding is continued with a constant injection bottom hole pressure of 3200 psi (the minimum pressure required for the production well) and a constant water rate of 300 bbl/day. The recovery factor increased to around 0.63 as shown in the figure.

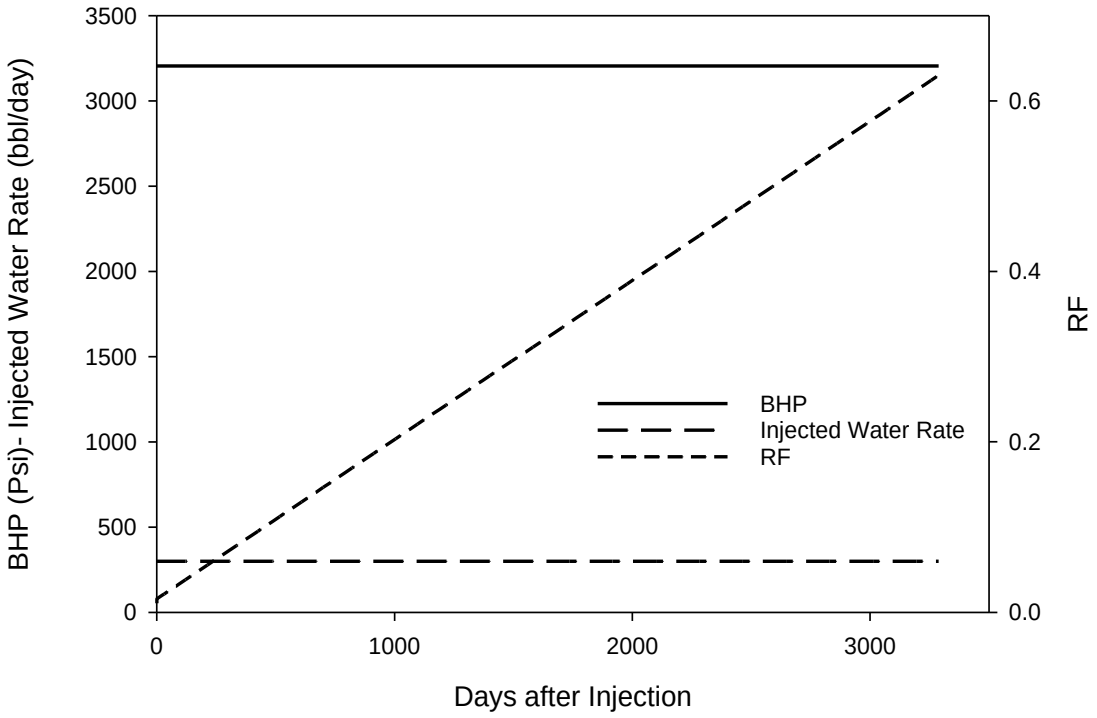

Figure 4- 8: Recovery factor without considering the impact of scaling. A recovery factor up to 0.63 can be achieved when the effect of scaling issue on the reservoir formation is not included.

In the second scenario, the chemical reactions during water flooding were considered and the results were plotted in Figure 4- 9. As can be seen, the injection pressure started to increase continuously from the beginning of the flooding process until it reached the maximum bottom hole pressure that was enforced on the injection well. The water rate

was constant in this duration and recovery factor increased. However, as the pressure reached the maximum pressure condition, water rate started to drop and as a result, recovery factor tended to increase with a smaller slope. The final recovery factor achieved in this case was around 0.35, which is less than the first case.

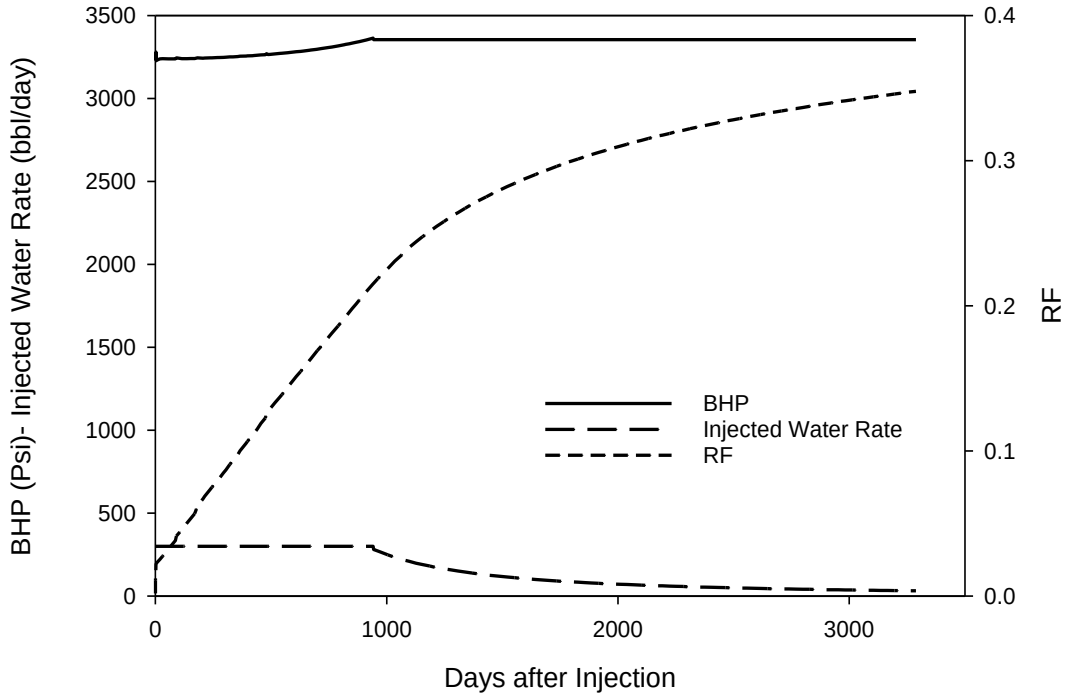

Figure 4- 9: Recovery factor with including the impact of scale formation on reservoir porous media. Recovery factor decreases as a result of scaling issue. The bottom hole pressure tends to increase to overcome the precipitations until it reaches the maximum bottom hole pressure enforced on the injection well. Once the maximum bottom hole pressure is reached, the injection water rate starts to decrease leading in a smaller recovery factor.

The maximum bottom hole pressure for the injection well was increased from 3355 psi to 3555 psi to see how much it will mitigate the effect of scaling on recovery factor. The results are shown in Figure 4- 10. As can be observed, the recovery factor has increased in this case as the bottom hole pressure was allowed to increase from the minimum pressure for supporting the production up to 3555 psi. This led in an increase in the

recovery factor as a higher injection pressure causes more production as verified by the results. In addition, it can be noted that the water injection drop is delayed until the later stages of flooding which leads in a higher recovery factor.

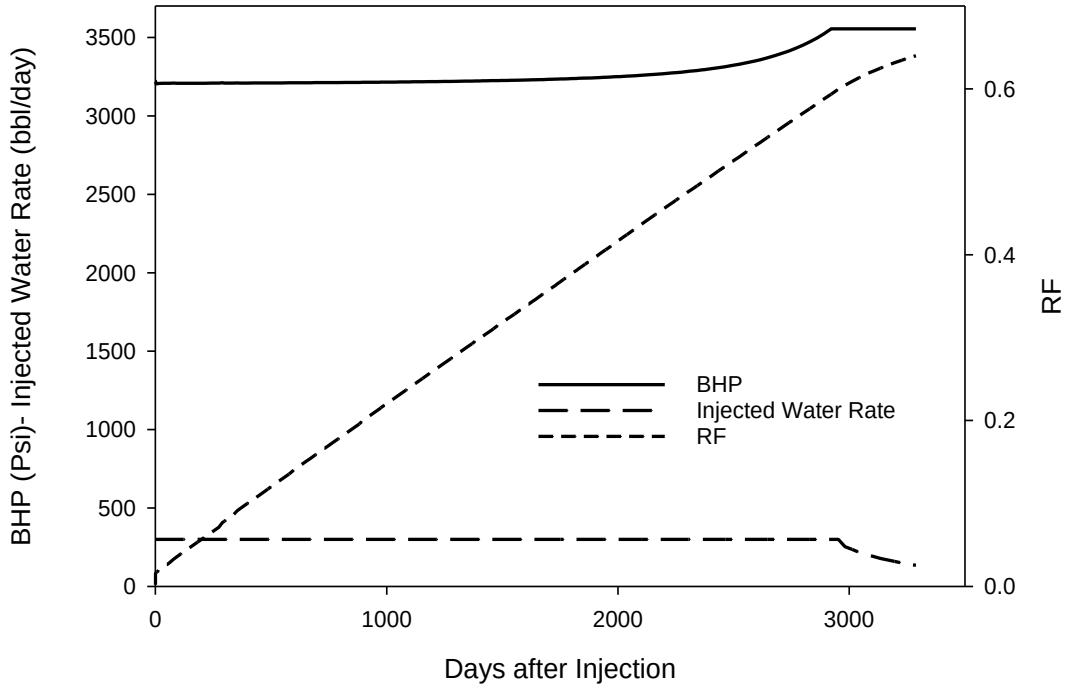

Figure 4- 10: Impact of maximum bottom hole pressure on recovery factor. Assigning a larger maximum bottom hole pressure leads in a larger recovery factor when scaling causes formation damage.

4.6: Composite $BaSO_4$-$CaSO_4$ Scaling

4.6.1: Impact of Composite $BaSO_4$-$CaSO_4$ Scaling on Reservoir Performance

In this part of the study, calcium sulfate was added to barium sulfate (barite) to investigate the impact of composite scale formation on the water flooding performance. In one case, only barite was considered as the scaling agent and in the other case, both barite and calcium sulfate were considered as the occurring scale formations. The

kinetic information of calcium sulfate was collected from the literature [59]. Other parameters were the same as before. The amounts of barite precipitation and porosity reduction for the first case are shown in Figure 4- 11 and**Error! Reference source not found.** Figure 4- 12. The results for the composite case are shown in Figure 4- 13, Figure 4- 14 and Figure 4- 15. As can be observed, the composite scale has a smaller impact on the reservoir porosity reduction. In fact, the presence of calcium ions prevents the sulfate ions to completely react with barium ions and form barium sulfate. Therefore, some of the sulfate ions react with the calcium ions. This leads in a less amount of barite precipitation as shown in Figure 4- 13 and precipitation of calcium sulfate as shown in Figure 4- 14. Although calcium sulfate precipitation is added to barite precipitation, the combined scale leads in a less damage on the reservoir.

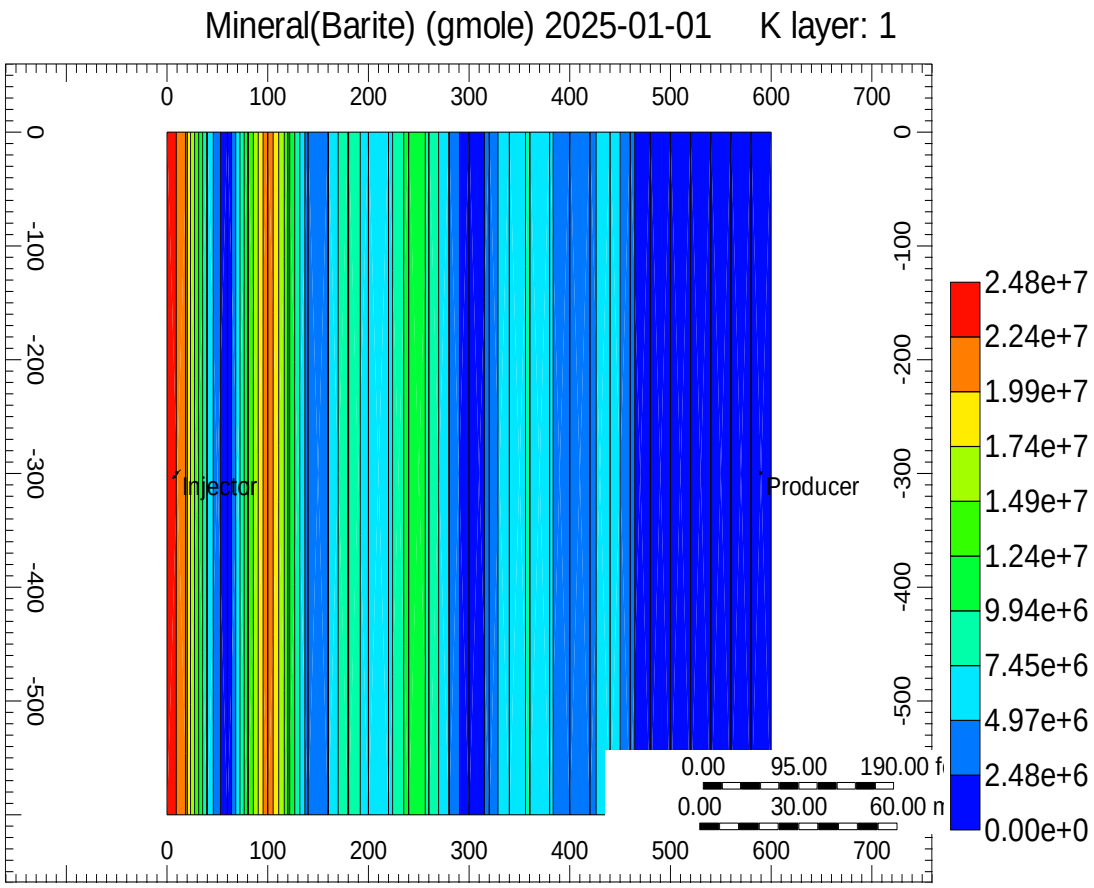

Figure 4- 11: Amount of barite precipitation when barite is the only scaling agent in the reservoir. The amount of barite precipitation is largest closer to the injection well and decreases by moving towards the production well.

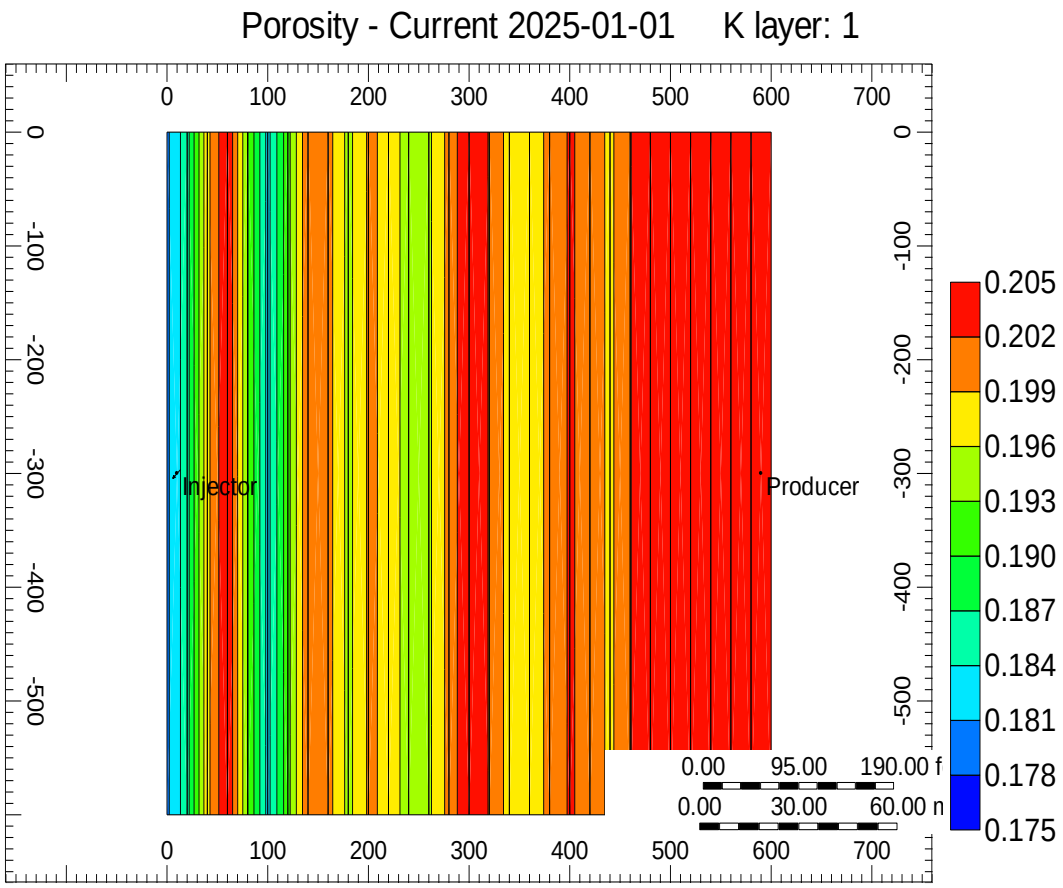

Figure 4- 12: Porosity profile when only barite scaling exists in the reservoir. Porosity reduction is largest closer to the injection well and decreases by moving towards the production well.

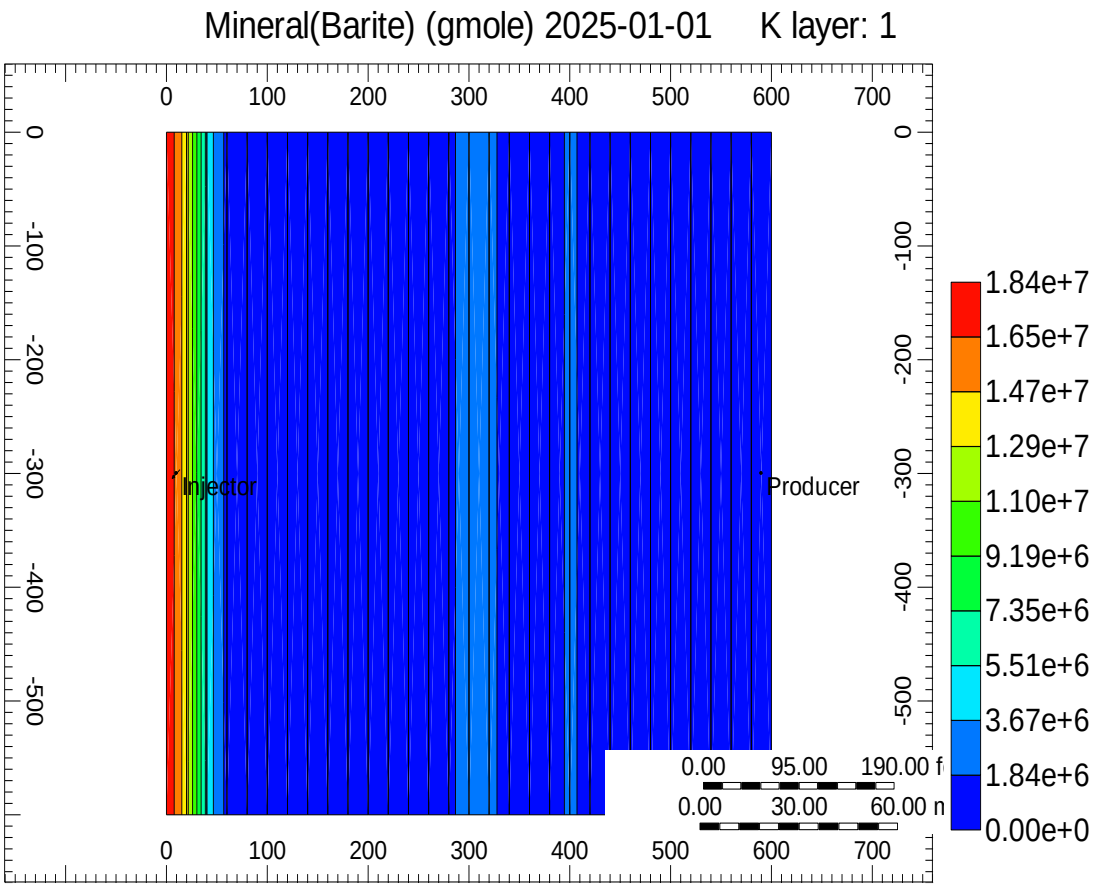

Figure 4- 13: Amount of barite precipitation when barite and $CaSO_4$ are the scaling agents in the reservoir. Barite precipitation decreases as less sulfate ions are provided for the barium cations when calcium ions exist in the reservoir.

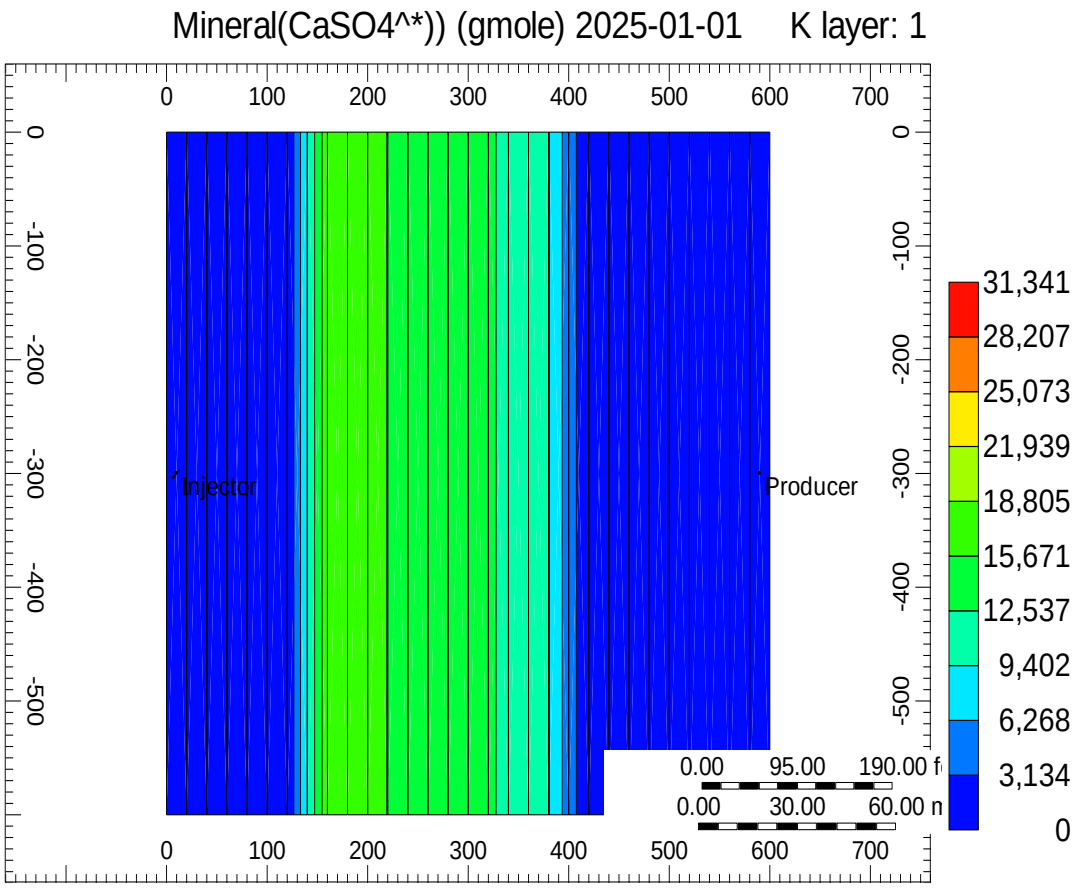

Figure 4- 14: Amount of $CaSO_4$ precipitation when composite $BaSO_4$- $CaSO_4$ occurs in the reservoir. Some of sulfate inions are removed from the reservoir by the calcium cations and this leads in an increase in the calcium sulfate precipitation while it causes a decrease in barite precipitation.

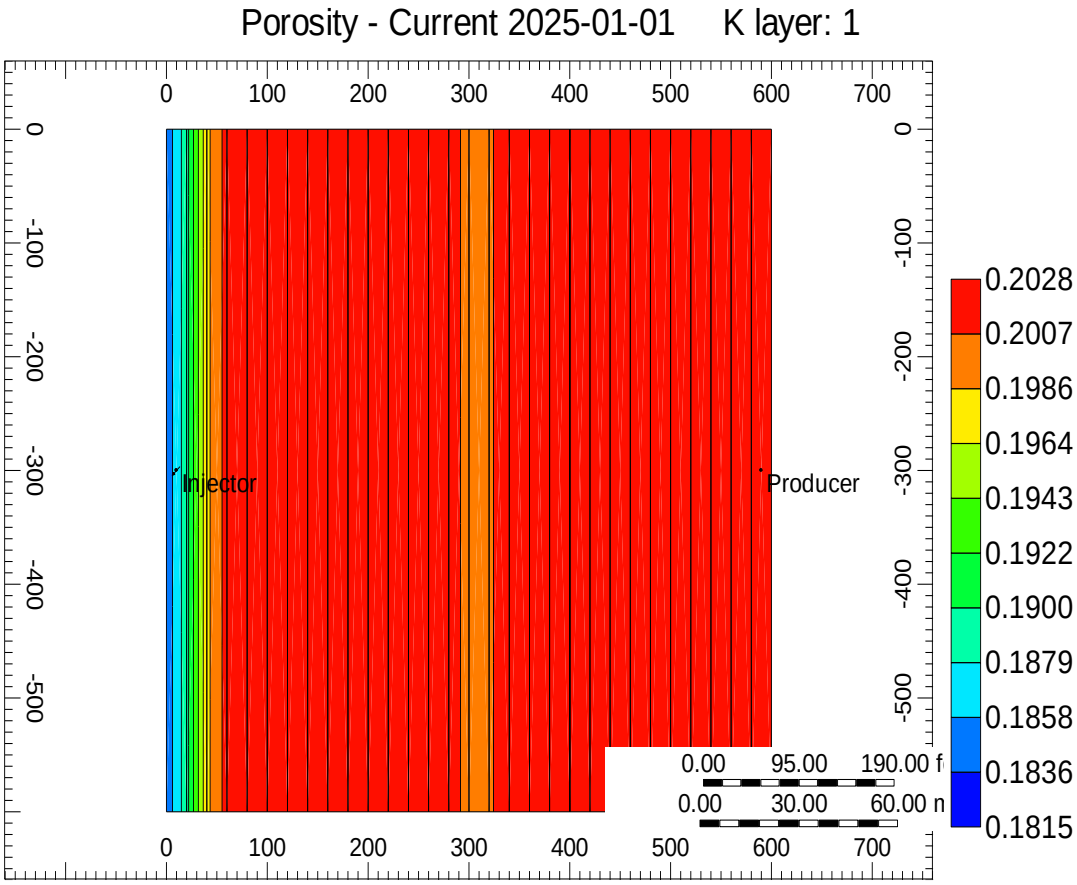

Figure 4- 15: Porosity reduction as a result of composite $BaSO_4$- $CaSO_4$ scaling. Porosity reduction is less compared to the case in which only barite precipitation exists. In addition, most of the reduction occurs closer to the injection well.

4.6.2: Impact of Composite $BaSO_4$-$CaSO_4$ Scaling on Injection Performance

In order to investigate the impact of composite scale on well performance, the bottom hole pressure of the injection well was plotted in Figure 4- 16 for both single barite scale and composite $BaSO_4$-$CaSO_4$ scale. As can be observed, the composite scale has a less negative impact on the injection performance as it requires a smaller injection pressure for maintaining the same production rate.

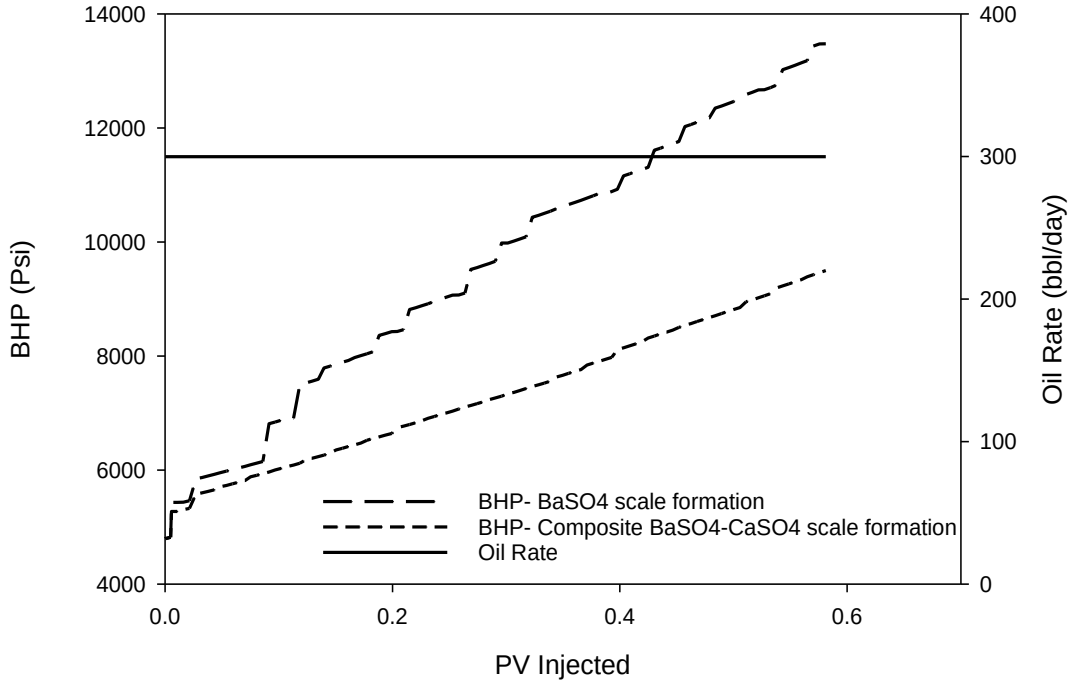

Figure 4- 16: Impact of composite $BaSO_4$- $CaSO_4$ scaling on well performance. Composite scaling has a less impact on the injection pressure required for the constant production.

4.7: The impact of In-Situ Scale Formation on Waterflooding Performance from the Saturation Profiles Outlook

4.7.1: Evaluation of Waterflooding Performance

Water flooding performance is usually evaluated by means of saturation profiles. An ideal water flooding operation or piston-like displacement is one in which the mobility ratio of the displacing fluid and the displaced fluid is less than unity. In this case, the water flooding is performed in a piston like fashion similar to the following figure:

Figure 4- 17: Ideal water flooding - Piston like displacement of a 1D model with one injector on the left and on producer on the right.

However, in most cases, many factors such as reservoir heterogeneity, capillarity, and dispersivity make the displacement non- ideal and therefore the efficiency of the water flooding operation is reduced. When the mobility ratio is greater than unity, the displacing fluid bypasses the displaced fluid and the displacement deviates from ideal behavior. The following figure demonstrates a typical non- ideal behavior:

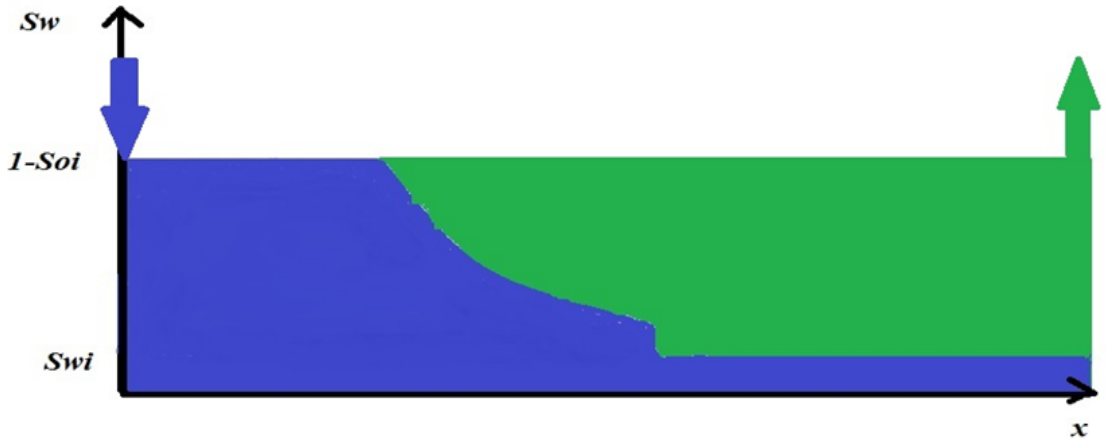

Figure 4- 18: Non-ideal water flooding- The tongues of the displacing fluid (water) are bypassing the displaced fluid (oil).

When the displacement is not ideal, the saturation profile is predicted by the by the Buckley Leverett theory [60-62].

In order to investigate the impact of chemical reactions on the saturation profile of the injected water, a one-dimensional model including 100 grid blocks was considered. Each grid block was 6 ft. in length and 150 ft. in height. The width of the reservoir was considered 600 ft. Other properties of the reservoir and the fluids were considered the same as discussed before. The reason behind selection of the 1D model is to simplify the process to be able to put the main focus on the saturation profiles of the injected water. The concentrations of barium, sulfate and barite as well as the corresponding porosity reduction as a result of the injection of sulfate into the 1D barium rich formation water are illustrated in Figure 4- 19. As can be observed, the porosity can decrease up to .077 in some locations.

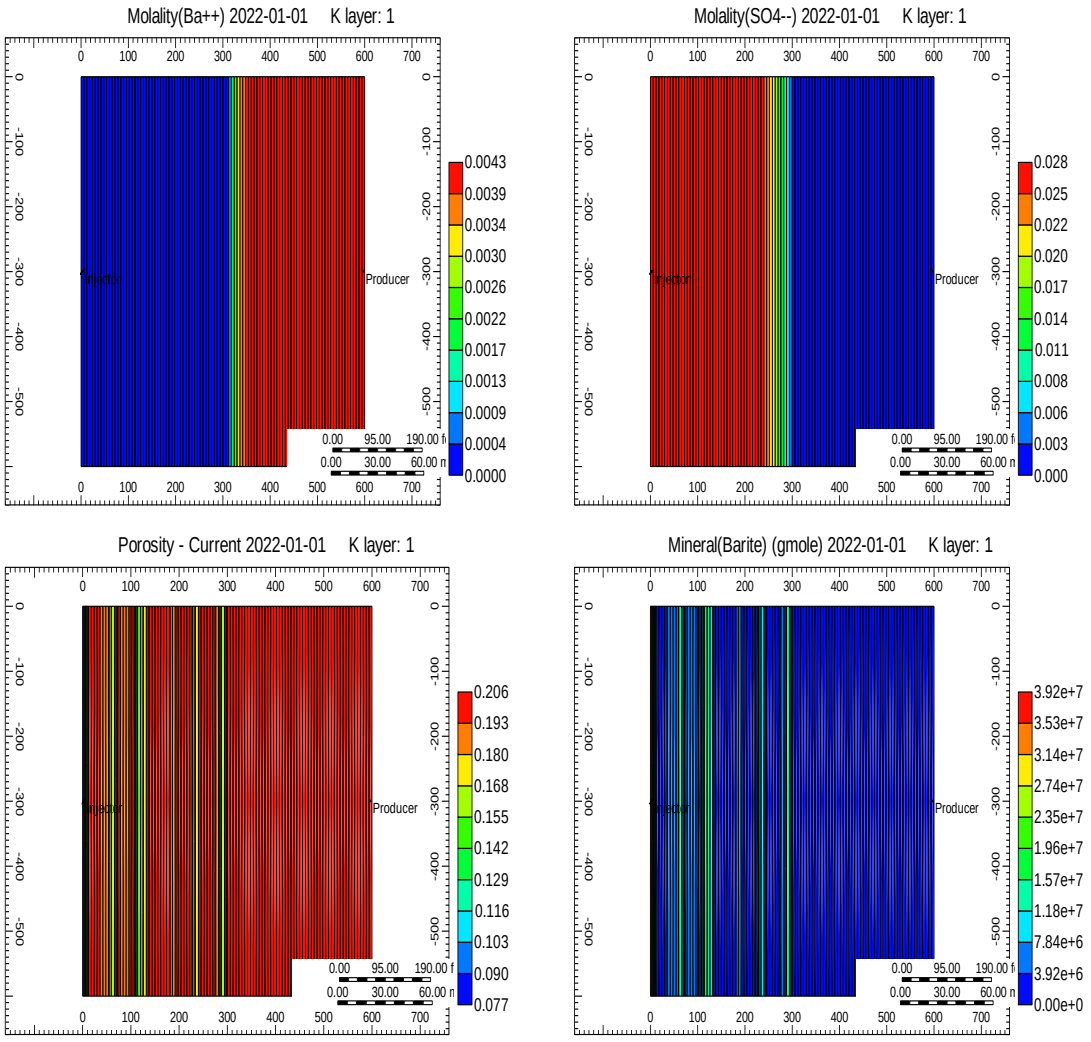

Figure 4- 19: Profile of barium, sulfate and barite concentrations and the corresponding porosity reduction after six years of water flooding, 0.4 PV injected. Injection of sulfate into the barium rich formation leads in porosity reduction up to 0.077.

In order to investigate the impact of scale formation on saturation profiles, two simulation scenarios were performed. In one scenario, water flooding was performed without considering the chemical reactions and the saturation profiles at different injected pore volumes are plotted in Figure 4- 20. As can be seen in this figure, the

performance of the water flooding is very close to the piston like behavior during the water flooding operation without including the impact of in situ scale formation. In the second case, the scaling issue resulting from the single barite precipitation in the reservoir was considered during the flooding operation and the results are illustrated in the same figure. As can be seen from the plots, the water flooding performance is deviating from the piston like behavior. In addition, it can be concluded from the scaling plots that the chemical reactions cause earlier water breakthroughs, which is not favored during water flooding. The reason behind these phenomena is in fact related to the relative permeabilities of the water and oil phases in the fractional flow equations and the formation porosity that decreases because of scale deposition. Another conclusion can be drawn from this figure: The performance of water flooding becomes less efficient at the later times of flooding because of barite scale formation. From a quantitative standpoint, it can be observed from the figure that scaling issue leads in earlier water breakthroughs for up to 60 ft., which can affect the efficiency of the water-flooding project.

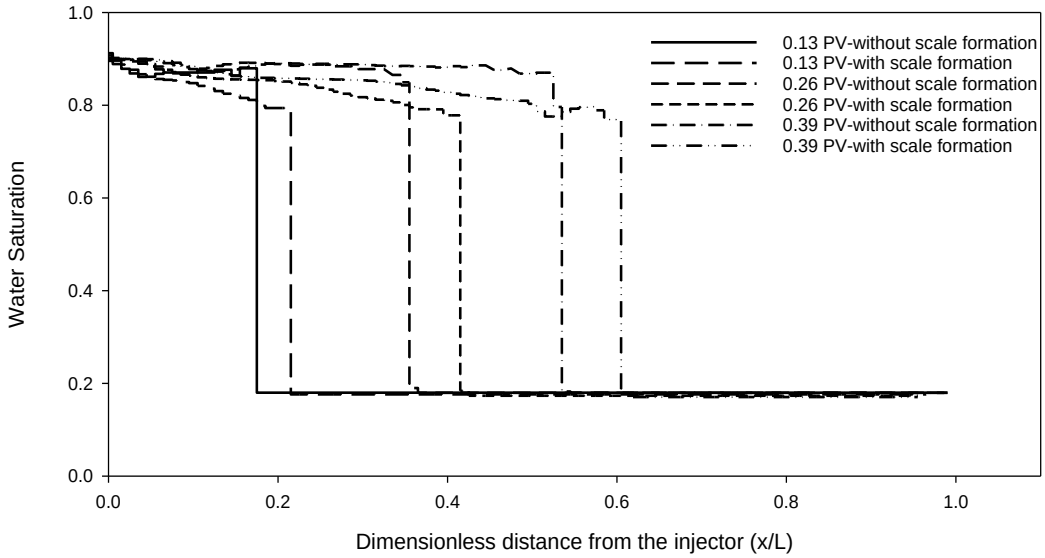

Figure 4- 20: The impact of scale formation on the saturation profile during water flooding. The mineral deposition makes the saturation profiles deviate from ideal behavior and leads in an earlier water breakthrough.

4.7.2: Sensitivity Analysis based on the Reactive Surface Area of Barite

As it was mentioned before, reactive surface area plays an important role in determining the amount of precipitation/dissolution. Here, a sensitivity analysis based on the reactive surface area of the barite mineral during incompatible water flooding was performed.

The sensitivity analysis was performed at different injected pore volumes to capture the impact of reactive surface area on the water flooding performance. In one case, the reactive surface area of the barite was assumed 90 m^2/m^3 of bulk volume of rock and in the second case, this value was assumed 900 m^2/m^3. The results of this comparison are illustrated in Figure 4- 21. As can be observed, a larger reactive surface area, which leads in more barite precipitation, causes a more non-ideal behavior and an earlier

breakthrough which both are not favored during water-flooding. These results infer that more precipitations cause displacement problems during water flooding. It should be pointed out that the injected pore volume and reactive surface area are independent. In other words, only one of the rates in Figure 4- 21 was sufficient for conducting the sensitivity analysis. However, we have added three different pore volumes to investigate the impact of scale formation and reactive surface at different stages of flooding.

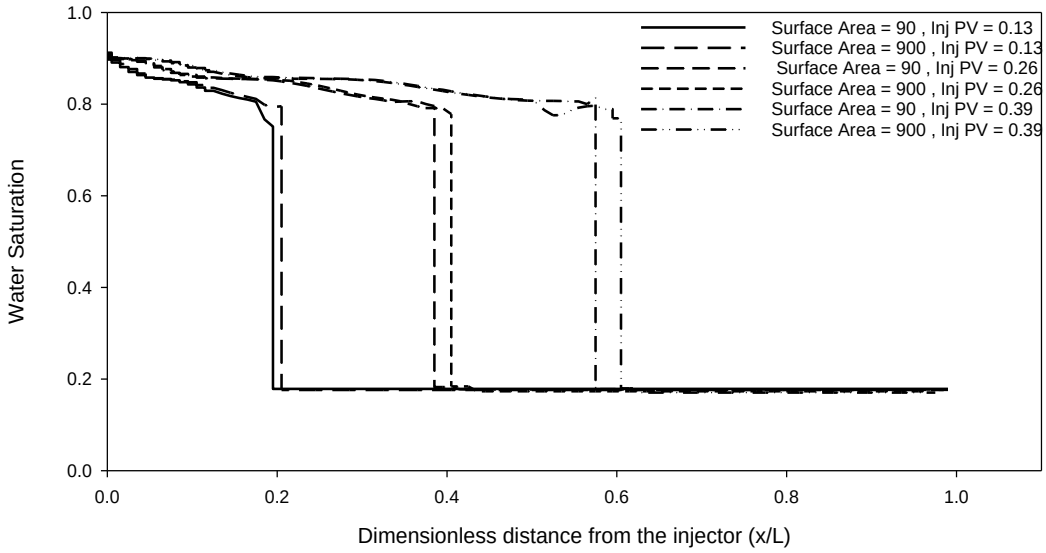

Figure 4- 21: Sensitivity analysis based on the reactive surface area of barite at different injected pore volumes. A larger reactive surface area leads in more precipitation and consequently a larger impact on the water flooding performance.

4.8: Summary

The principal geochemical processes that lead in scale formation and formation damage were presented. In addition, a brief description of barite scale deposition and reactive surface area of minerals was provided. Sensitivity analysis based on the reactive surface

area of barite shows that a larger surface area leads in a less efficient water flooding operation.

A base case model was made for investigating scale formation during water flooding. To this end, seawater with a real water composition from the literature was considered for injection into a reservoir in which the formation water composition was also collected from a real case. Simulations were run for two scenarios: In one scenario, atypical water flooding process was designed and in the second case, the geochemical reactions that lead in scale formation within the reservoir were taken into consideration. The impact of scale formaton on reservoir properties was also studied. Scale formation can decrease the reservoir porosity from an initial value of 0.2 to a final value of 0.08.

The impact of scale formation on injection performance and oil recovery was investigated in this chapter as well. The required bottom hole pressure for a constant production rate increases when scale forms within the reservoir. Larger reactive surface area leads in a higher bottom hole pressure required for constant production. Scale formation also leads in less oil recovery compared to the case in which the impact of scale formation is neglected.

Calcium sulfate was added to barium sulfate to study the effect of composite scale formation on reservoir properties and injection performance. Composite barite/calcium sulfate scaling causes less damage on the reservoir performance compared to the case of single barite scale.

The impact of barite scale formation on water flooding efficiency was studied. The efficiency of water flooding in terms of Ideal and non-ideal displacement behavior was

quantified by means of water saturation profiles. Scale formation leads in non-ideal water flooding displacement and the performance of water flooding becomes less efficient at the later times of flooding.

Chapter 5: Summary, Conclusions and Recommendations

5.1: Summary

Mineral scale formation in reservoir formation during water flooding was studied in this research. A robust model was developed for predicting permeability damage resulting from scale formation in reservoir porous media. In addition, the developed model was coupled with Carman-Kozeny equation to develop a modified relationship between porosity and permeability of porous media affected by mineral deposition.

Barium sulfate was considered as the main scaling agent in reservoir porous media by injecting seawater rich in sulfate into a formation rich in barium. Detailed mechanisms of scale formation and formation damage were examined throughout the work and the impact of scale deposition inside the reservoir on reservoir performance was thoroughly studied.

Water saturation profiles before and after scale formation were examined and the impact of scale formation on the efficiency of water flooding operation was assessed.

Calcium sulfate was added to barium sulfate and the impact of composite scale formation on injection performance and reservoir properties were studied.

5.2: Conclusions

The following detailed conclusions can be drawn from this work:

- The developed model for prediction of formation damage resulting from scale deposition was found to be accurate and robust. The results of average absolute percentage relative error (AAPRE) showed that the high concentration model predicts permeability damage ratio with an AAPRE of 0.889% and the normal concentration model predicts the damage ratio at with an AAPRE of 0.427%. In addition, the coefficient of determination (R^2) was found to be 0.948 and 0.941 for the first and second model, respectively. Error distribution curves showed that the models are consistent in estimating permeability damage with high accuracy over a wide range of input parameters. Relevancy factor indicated that the volume of injected incompatible water has the greatest impact on permeability reduction caused by scaling issue.
- Injection of seawater rich in sulfate into a formation rich in barium causes the mixed fluid to precipitate barite. Barite scale formation significantly affects the reservoir performance. Porosity can decrease from 0.2 to 0.08 because of scale formation.
- Scale formation causes the water flooding behavior to deviate from ideal displacement to non-ideal displacement. In addition, a larger reactive surface area of barite leads in a less efficient injection. The impact of scale formation on water flooding efficiency is more severe in the later stages of flooding.
- Scale formation leads in a higher bottom hole pressure required for injection when a constant production rate is favored. In addition, oil recovery drops because of scale formation when a larger production is favored.

- Composite barium sulfate/calcium sulfate scaling causes less damage to the reservoir properties and injection performance. The reason behind is the removal of sulfate anions by the calcium cations when both calcium and barium ions exist in the formation water.

5.3: Recommendations for Future Work

The following recommendations may be considered for future research:

- A more general pore structure for the porous media and a nonuniform distribution for the thickness of deposition in the pore bodies can be considered for developing a model that captures the heterogeneity of porous media.
- Calcium carbonate can be added to the system to investigate the impact of co-precipitation of carbonate and sulfate scales on reservoir performance.
- Scale formation can occur during CO_2 injection and sequestration processes as well. The impact of scale precipitation during the mentioned operations can be investigated by employing a similar approach presented in this research.
- Scale formation and its impact on reservoir performance and water injection have been thoroughly studied in this work. Next step should focus on developing a method to overcome the issues caused by scale formation that were mentioned in this study.

Bibliography

1. *Moghadasi, J., et al. Formation damage due to scale formation in porous media resulting from water injection. in SPE International Symposium and Exhibition on Formation Damage Control. 2004. Society of Petroleum Engineers.*

2. *Merdhah, M. and A. Badr, The study of scale formation in oil reservoir during water injection at high-barium and high-salinity formation water. 2008, Universiti Teknologi Malaysia, Faculty of Chemical and Natural Resources Engineering.*

3. *Ahmed, S.J., Laboratory study on precipitation of calcium sulphate in berea sandstone cores. 2004, Citeseer.*

4. *Wat, R., et al. Kinetics of BaSO4 crystal growth and effect in formation damage. in SPE Formation Damage Control Symposium. 1992. Society of Petroleum Engineers.*

5. *McElhiney, J.E., et al. Determination of in-situ precipitation of barium sulphate during coreflooding. in International Symposium on Oilfield Scale. 2001. Society of Petroleum Engineers.*

6. *Naseri, S., J. Moghadasi, and M. Jamialahmadi, Effect of temperature and calcium ion concentration on permeability reduction due to composite barium and calcium sulfate precipitation in porous media. Journal of Natural Gas Science and Engineering, 2015.* ***22****: p. 299-312.*

7. *Vetter, O., V. Kandarpa, and A. Harouaka, Prediction of scale problems due to injection of incompatible waters. Journal of Petroleum Technology, 1982.* ***34****(02): p. 273-284.*

8. *Tahmasebi, H.A., R. Kharrat, and M. Soltanieh, Dimensionless correlation for the prediction of permeability reduction rate due to calcium sulphate scale deposition in carbonate grain packed column. Journal of the Taiwan Institute of Chemical Engineers, 2010.* ***41****(3): p. 268-278.*

9. *Putnis, A., Transient porosity resulting from fluid–mineral interaction and its consequences. Rev Mineral Geochem, 2015.* ***80****: p. 1-23.*

10. *Peysson, Y., et al., Permeability alteration due to salt precipitation driven by drying in the context of CO 2 injection. Energy Procedia, 2011.* ***4****: p. 4387-4394.*

11. *Read, P.A. and J.K. Ringen. The use of laboratory tests to evaluate scaling problems during water injection. in SPE Oilfield and Geothermal Chemistry Symposium. 1982. Society of Petroleum Engineers.*

12. *Ghaderi, S., R. Kharrat, and H. Tahmasebi, Experimental and theoretical study of calcium sulphate precipitation in porous media using glass micromodel. Oil & Gas Science and Technology-Revue de l'IFP, 2009.* ***64****(4): p. 489-501.*

13. *Li, L., C.A. Peters, and M.A. Celia, Upscaling geochemical reaction rates using pore-scale network modeling. Advances in water resources, 2006.* ***29****(9): p. 1351-1370.*

14. *Zeidouni, M., M. Pooladi-Darvish, and D. Keith. Sensitivity Analysis of Salt Precipitation and CO2-Brine Displacement in Saline Aquifers. in SPE International Conference on CO2 Capture, Storage, and Utilization. 2009. Society of Petroleum Engineers.*

15. *Kan, A., et al. Validation of Scale Prediction Algorithms at Oilfield Conditions. in SPE International Symposium on Oilfield Chemistry. 2005. Society of Petroleum Engineers.*

16. *Yeboah, Y., S. Somuah, and M. Saeed. A new and reliable model for predicting oilfield scale formation. in SPE International Symposium on Oilfield Chemistry. 1993. Society of Petroleum Engineers.*

17. *Bertero, L., et al., Chemical equilibrium models: their use in simulating the injection of incompatible waters. SPE Reservoir Engineering, 1988.* ***3****(01): p. 288-294.*

18. *Thomas, L., et al. Chemical characterization of fluids and their modelling with respect to their damage potential in injection on production processes using an expert system. in SPE International Symposium on Oilfield Chemistry. 1995. Society of Petroleum Engineers.*

19. *Moghadasi, J., et al. Formation damage in Iranian oil fields. in International Symposium and Exhibition on Formation Damage Control. 2002. Society of Petroleum Engineers.*

20. *Crabtree, M., et al., Fighting scale—removal and prevention.*

21. *Fadairo, A., O. Omole, and O. Falode, A Modified Model for Predicting Permeability Damage due to Oilfield Scale Deposition. Petroleum Science and Technology, 2009.* ***27****(13): p. 1454-1465.*

22. *Application of ARIMA and GARCH Models in Forecasting the Natural Gas Prices.*

23. *Agarwal, S., H.R. Saferpour, and C.H. Dagli, Adaptive learning model for predicting negotiation behaviors through hybrid k-means clustering, linear vector quantization and 2-Tuple fuzzy linguistic model. Procedia Computer Science, 2014.* ***36****: p. 285-292.*

24. *Hosseinipoor, S., Gas-Solid Catalytic Reaction Modeling and Its Computational Solution. 2001, Amirkabir University of Technology.*

25. *Hosseinipoor, S., Forecasting Natural Gas Prices in the United States Using Artificial Neural Networks. 2016, University of Oklahoma.*

26. *Kamali, A. and M. Pournik, Fracture closure and conductivity decline modeling–Application in unpropped and acid etched fractures. Journal of Unconventional Oil and Gas Resources, 2016.* ***14****: p. 44-55.*

27. *Omidvar, A., M. Garakani, and H.R. Safarpour, Context based user ranking in forums for expert finding using WordNet dictionary and social network analysis. Information Technology and Management, 2013: p. 1-13.*

28. *Safarpour, H.R., et al., Single Supply of Electrical Energy in the Supply Distribution Model: Using Gams to Model the Effects of Network Parameters on the Level of Consumer Demand. International Journal of Research in the Academic Disciplines in Higher Education, 2013.*

29. *Safari, H. and M. Jamialahmadi, Estimating the kinetic parameters regarding barium sulfate deposition in porous media: a genetic algorithm approach. Asia-Pacific Journal of Chemical Engineering, 2014.* ***9****(2): p. 256-264.*

30. *Safari, H., et al., Prediction of the aqueous solubility of BaSO 4 using pitzer ion interaction model and LSSVM algorithm. Fluid Phase Equilibria, 2014.* ***374****: p. 48-62.*

31. *Merdhah, A.B. and A. Yassin, Formation damage due to scale formation in porous media resulting water injection. system, 2008.* ***14****: p. 15.*

32. *Moghadasi, J., et al. Scale formation in oil reservoir and production equipment during water injection (Kinetics of CaSO4 and CaCO3 crystal growth and effect on formation damage). in SPE European Formation Damage Conference. 2003. Society of Petroleum Engineers.*

33. *Moghadasi, J., et al. Scale formation in Iranian oil reservoir and production equipment during water injection. in International Symposium on Oilfield Scale. 2003. Society of Petroleum Engineers.*

34. *Moghadasi, J., et al., Model study on the kinetics of oil field formation damage due to salt precipitation from injection. Journal of Petroleum Science and Engineering, 2004.* ***43****(3): p. 201-217.*

35. *Chang, F. and F. Civan, Practical model for chemically induced formation damage. Journal of Petroleum Science and Engineering, 1997.* ***17****(1): p. 123-137.*

36. *Muller, N., et al., CO2 injection impairment due to halite precipitation. Energy procedia, 2009.* ***1****(1): p. 3507-3514.*

37. *Mardia, K.V., J.T. Kent, and J.M. Bibby, Multivariate analysis. 1979: Academic press.*

38. *ÁÒ, Ô. and Ä. ØÝ, Multiple regression analysis. 1998.*

39. *Hair, J.F., Multivariate data analysis. 2010.*

40. *Hair, J.F., et al., Multivariate data analysis. Vol. 6. 2006: Pearson Prentice Hall Upper Saddle River, NJ.*

41. *Beautrelet, I. Derivation of the Least Squares Estimator for Beta in Matrix Notation. 2015; Available from: http://economictheoryblog.com/2015/02/19/ols_estimator/.*

42. *Dixon, W.J. and F.J. Massey, Introduction to statistical analysis. Vol. 344. 1969: McGraw-Hill New York.*

43. *Johnson, R.A. and D.W. Wichern, Applied multivariate statistical analysis. Vol. 4. 1992: Prentice hall Englewood Cliffs, NJ.*

44. *Blount, C., Barite solubilities and thermodynamic quantities up to 300 degrees C and 1400 bars. American Mineralogist, 1977.* ***62****(9-10): p. 942-957.*

45. *Hajirezaie, S., et al., A Smooth Model for the Estimation of Gas/Vapor Viscosity of Hydrocarbon Fluids. Journal of Natural Gas Science and Engineering, 2015.*

46. *Dullien, F.A., Porous media: fluid transport and pore structure. 2012: Academic press.*

47. *Lake, L.W., Enhanced oil recovery. 1989.*

48. *FLUID MECHANICS, TUTORIAL No.4, FLOW THROUGH POROUS PASSAGES. Available from: http://www.freestudy.co.uk/fluid%20mechanics/t4203.pdf.*

49. *Nghiem, L., et al. Modeling CO2 storage in aquifers with a fully-coupled geochemical EOS compositional simulator. in SPE/DOE symposium on improved oil recovery. 2004. Society of Petroleum Engineers.*

50. *Bethke, C.M., Geochemical and biogeochemical reaction modeling. 2007: Cambridge University Press.*

51. *Delany, J. and S. Lundeen, The LLNL Thermochemical Database, Lawrence Livermore National Laboratory Report. Lawrence Livermore National Laboratory Report: Livermore, CA, 1994.*

52. *Kharaka, Y.K., et al., SOLMINEQ. 88: A computer program for geochemical modeling of water-rock interactions. US Geological Survey Water-Resources Investigations Report, 1988.* ***88****(4227): p. 420.*

53. *Peters, C.A., Accessibilities of reactive minerals in consolidated sedimentary rock: An imaging study of three sandstones. Chemical Geology, 2009.* ***265****(1): p. 198-208.*

54. *Misra, K.C., Introduction to geochemistry: principles and applications. 2012: John Wiley & Sons.*

55. *Hubbard, C.G., et al., Isotopic insights into microbial sulfur cycling in oil reservoirs. Frontiers in microbiology, 2014.* ***5****.*

56. *Christy, A.G. and A. Putnis, The kinetics of barite dissolution and precipitation in water and sodium chloride brines at 44–85 C. Geochimica et Cosmochimica Acta, 1993.* ***57****(10): p. 2161-2168.*

57. *Noiriel, C., et al., Changes in reactive surface area during limestone dissolution: An experimental and modelling study. Chemical Geology, 2009.* ***265****(1): p. 160-170.*

58. *Luo, S., R. Xu, and P. Jiang, Effect of reactive surface area of minerals on mineralization trapping of CO2 in saline aquifers. Petroleum Science, 2012.* ***9****(3): p. 400-407.*

59. *Palandri, J.L. and Y.K. Kharaka, A compilation of rate parameters of water-mineral interaction kinetics for application to geochemical modeling. 2004, DTIC Document.*

60. *Ayatollahi, S., EOR. 2011.*

61. *Devegowda, D., Waterflooding - I. 2012.*

62. *Green, D.W. and G.P. Willhite, Enhanced oil recovery. 1998: Richardson, Tex.: Henry L. Doherty Memorial Fund of AIME, Society of Petroleum Engineers.*